PEDF-Rpsa-Itga6 signaling regulates cortical neuronal morphogenesis

Short title: Rpsa regulates neuromorphogenesis

Sara M. Blazejewski, Sarah A. Bennison, Ngoc T. Ha, Xiaonan Liu, Trevor H. Smith, Kimberly J. Dougherty, and Kazuhito Toyo-oka*

Department of Neurobiology and Anatomy, Drexel University College of Medicine

Philadelphia, PA 19129 USA

Corresponding Author*

Kazuhito Toyo-oka, Ph.D.

Department of Neurobiology and Anatomy

Drexel University College of Medicine

2900 W Queen Lane, Room 186, Philadelphia, PA 19129 USA

Email: kt469@drexel.edu

Phone: (215) 991-8288

Fax: (215) 843-9082

Abstract

Neuromorphological defects underlie neurodevelopmental disorders and functional defects. We identified a function for ribosomal protein SA (Rpsa) in regulating neuromorphogenesis using *in utero* electroporation to knockdown Rpsa, which results in apical dendrite misorientation, fewer/shorter extensions with decreased arborization, and decreased spine density with altered spine morphology. We investigated Rpsa's ligand, pigment epithelium-derived factor (PEDF), and interacting partner on the plasma membrane, Integrin subunit α6 (Itga6). Rpsa, PEDF, and Itga6 knockdown cause similar phenotypes, with Rpsa and Itga6 overexpression rescuing morphological defects in PEDF deficient neurons *in vivo*. Additionally, Itga6 overexpression facilitates Rpsa expression on the membrane. GCaMP6s was used to functionally analyze Rpsa knockdown via *ex vivo* calcium imaging. Rpsa deficient neurons showed less fluctuation in fluorescence intensity, suggesting defective sub-threshold calcium signaling. Our study identifies a role for PEDF-Rpsa-Itga6 signaling in neuromorphogenesis, thus implicating these molecules in the etiology of neurodevelopmental disorders and identifying them as potential therapeutic candidates.

Author Summary

Investigating the mechanisms that drive neuromorphogenesis is a crucial step towards understanding normal and disordered brain development. We found that Rpsa signaling, which is facilitated by Rpsa's ligand PEDF and its plasma membrane interaction partner Itga6, regulates several key aspects of neuronal morphogenesis including dendritogenesis and dendritic spine formation. We also found that PEDF-Rpsa-Itga6 signaling contributes to calcium signaling, which is important for neuronal function. Furthermore, overexpression of Itga6 increased the expression of Rpsa on the plasma membrane, where it binds extracellular ligands, suggesting that Itga6 facilitates Rpsa signaling in this manner. Thus, PEDF, Rpsa, and Itga6 are implicated in the etiology of neurodevelopmental disorders. This work is of particular relevance to Miller-Dieker syndrome. The PEDF gene (*Serpinf1*) is located within a clinically relevant region of chromosome 17p13.3 that is deleted in Miller-Dieker syndrome patients. Severe lissencephaly, developmental delay, intellectual disability, and seizures are features of Miller-Dieker syndrome. Further investigation of PEDF-Rpsa-Itga6 signaling may increase our understanding of the mechanisms that contribute to MDS pathogenesis.

45 **Introduction**

46 Neuronal morphogenesis transforms an immature spherical neuron into a mature neuron
47 with a complex structure. Investigation of the mechanisms that drive neuromorphogenesis has
48 clear applications for improving treatments for neurodevelopmental disorders, as improper
49 neurite formation and dendritic development have been strongly associated with mental
50 retardation disorders and autism spectrum disorder (1-5). Inappropriate dendritic arborization
51 may also impact inputs and signaling efficiency between the synapse and soma (6, 7). Cortical
52 pyramidal neurons have one apical dendrite, which typically extends directly towards the cortical
53 plate. Apical dendrite orientation is crucial in determining synaptic connectivity and is important
54 for neuronal function, as misorientation of the apical dendrite could cause formation of aberrant
55 connections (8). The density and morphology of dendritic spines is another important aspect of
56 neuromorphogenesis. Dendritic spines are the site of over 90% of excitatory synapses in the
57 central nervous system (9). Spine morphology directly relates to synapse function and altered
58 spine phenotypes can result from neurodevelopmental disrders (10, 11).

59 Ribosomal protein SA (Rpsa), also known as the 67-kDa laminin receptor, functions in a
60 variety of roles including cell anchoring via laminins, ribosomal biogenesis, and chromatin and
61 histone binding (12). Mature Rpsa is embedded in the plasma membrane and may be
62 concentrated in lipid rafts, suggesting it functions as part of a signaling complex (13). Rpsa's
63 role as a laminin receptor has been extensively studied, revealing its importance in interacting
64 with the extracellular matrix (12, 14-16). Additionally, Rpsa initiates signaling for protection
65 against cell death induced by serum withdrawal in Neuroscreen-1 cells upon treatment with
66 laminin-1, demonstrating an important role for Rpsa in a neuron-like cell line (17). However, the
67 specific role of Rpsa in cortical development remains unknown.

68 Rpsa binds the secreted glycoprotein pigment epithelium-derived factor (PEDF) (18).
69 PEDF has neurotrophic properties and protects neurons in a variety of regions throughout the
70 central nervous system against excitotoxicity and oxidative damage (19). Recently, PEDF has
71 been shown to promote axon regeneration and functional recovery in dorsal root ganglion
72 neurons after spinal cord injury (20). PEDF expression declines with age and is downregulated
73 by more than 100-fold in aged human fibroblast as compared to young human fibroblast,
74 suggesting an important role for PEDF in early development (21). Additionally, *Serpinf1*, coding
75 for the PEDF protein, is encoded in a clinically relevant region of chromosome 17p13.3 known
76 as the Miller-Dieker Syndrome critical region that is frequently deleted or duplicated in a variety
77 of neurodevelopmental disorders (22, 23). Thus, the relationship between PEDF and its receptor
78 Rpsa in the developing cortex is of interest.
79 Binding of PEDF to Rpsa may involve a receptor complex that includes the integrin
80 subunit α6 (Itga6), which binds to the β4 subunit to form a complete integrin. Co-localization of
81 Rpsa and Itga6 on the plasma membrane may result from initial co-localization of Rpsa and
82 Itga6 in cytoplasmic complexes, leading to trafficking to the membrane together (12, 24).
83 Furthermore, Rpsa and Itga6 expression may be co-regulated (25). The Rpsa-Itga6 complex is
84 hypothesized to have a role in regulating or stabilizing Rpsa's interaction with laminin,
85 suggesting that an interaction between Rpsa and Itga6 could be important for other signaling
86 mechanisms like PEDF-Rpsa signaling (Ardini et al., 1997).
87 We analyzed the functions of Rpsa in cortical neuronal development by performing *in*
88 *utero* electroporation at E15.5 to induce knockdown (KD) of Rpsa in layer 2/3 cortical pyramidal
89 neurons (26-28). We found that Rpsa deficient cells show defects in apical dendrite orientation,
90 initiation and elongation of dendrites, dendritic branching, and dendritic spine density and

91 morphology *in vivo*. Similar defects are observed following Rpsa knockdown, PEDF KD, and
92 Itga6 KD. Rpsa overexpression (OE) rescued morphological defects resulting from PEDF KD *in*
93 *vivo*, suggesting that PEDF initiates Rpsa signaling to regulate neuromorphogenesis. Itga6 OE
94 rescued dendrite formation deficits caused by PEDF KD and facilitated the expression of Rpsa
95 on the plasma membrane, indicating a role for Itga6 in the signaling mechanism. Additionally,
96 we show that morphological changes associated with Rpsa KD impact sub-threshold calcium
97 activity. Our study identifies functions of the PEDF-Rpsa-Itga6 signaling pathway in cortical
98 neuromorphogenesis and implicates this signaling pathway in the etiology of
99 neurodevelopmental disorders.

100 **Results**

101 **The Expression of Rpsa in the Developing Cerebral Cortex**

102 The expression pattern of Rpsa has not been previously investigated in the developing
103 brain. Therefore, it was unknown at which levels or developmental time-points Rpsa is
104 expressed, which should be established when investigating the function of Rpsa during
105 development. To quantify the expression of Rpsa protein levels in the developing cerebral
106 cortex, we performed Western blots using lysate of the cerebral cortex from embryonic day (E)
107 13.5 to P7 samples (Fig. 1A and B). The Rpsa protein is moderately expressed in the developing
108 cortex during early embryonic stages (E13.5) and then expression decreases, but persists to at
109 least P7. This suggests that Rpsa may be crucial at earlier embryonic stages. We also analyzed
110 the spatial distribution of the Rpsa protein by immunofluorescence using E18.5 brain sections
111 (Fig. 1C). Rpsa is expressed throughout all cortical layers and in the cytoplasm, but not the
112 nucleus at E18. Furthermore, staining of primary cortical neurons confirmed the expression of
113 Rpsa in neurons by staining with the neuronal marker, class III β-tubulin, showing that Rpsa is
114 highly concentrated in the soma and proximal extensions, but is not found in the nucleus or more
115 distal extensions (Fig. 1D). Therefore, functions of Rpsa that can be associated with these
116 cellular localizations, such as interacting with the extracellular matrix, are likely more important
117 at this time-point.

118 **Rpsa KD is associated with apical dendrite misorientation at P3 that can be rescued by**
119 **Rpsa OE**

120 KD efficiency of our Rpsa CRISPR construct was tested via Western Blot and the
121 knockdown efficiency was approximately 77% (Suppl. Fig. 1A and B). Genomic alteration by
122 Rpsa CRISPR was mainly accomplished by deletions, but cases of single nucleotide additions

123 were also observed (Suppl. Fig. 1 C and D). To further confirm Rpsa KD, we performed
124 immunocytochemistry to stain for Rpsa in primary cortical mouse neurons that were transfected
125 with Rpsa CRISPR. Neurons positive for Rpsa KD had significantly decreased fluorescence
126 intensity for the Rpsa marker, as compared with untransfected controls (Suppl. Fig. 1 E and F).

127 To investigate apical dendrite orientation, we performed *in utero* electroporation at E15.5
128 to induce a CRISPR/Cas9 mediated KD of Rpsa. The orientation of the apical dendrite is an
129 important feature of neuronal morphology, since the angle at which the apical dendrite extends
130 with respect to the cortical plate is important for neuronal connectivity. Conducting this analysis
131 at P3 allowed for easy identification of the apical dendrite, since neuronal morphology is
132 relatively simple at this stage. We found that Rpsa KD cells (34.2° ± 3.61) had a significantly
133 greater mean angle from the soma than the control CRISPR cells (14.1° ± 1.63) (Fig. 2A and B).
134 The frequencies for degree of angle in Rpsa KD cells were more broadly distributed across a
135 wider range from -30° to 30°, while angle measurements were closer to 0° and more narrowly
136 distributed in control CRISPR cells (Fig. 2C). This suggests that Rpsa deficient cells have apical
137 dendrites that are inappropriately positioned at an abnormal angle, which may lead to formation
138 of aberrant synapses. The Rpsa KD phenotype could be rescued by CRISPR-resistant wild-type
139 Rpsa OE (11.8° ± 1.13), resulting in a phenotype comparable to the control CRISPR + control
140 OE group (11.7° ± 1.25) (Fig. 2). The possibility of the phenotype being caused by an off-target
141 effect of the CRISPR is minimal, since the Rpsa KD phenotype was able to be rescued by
142 CRISPR-resistant Rpsa OE.

143 Additionally, we measured the length of the apical dendrite and found no significant
144 difference between Rpsa KD (27.7 μm ± 1.4) and control CRISPR (27.5 μm ± 1.6) (Suppl. Fig.
145 2). This suggests that there is no defect in the early period of dendrite elongation.

146 **Rpsa KD is associated with defects in neuronal morphogenesis at P15 that can be rescued**
147 **by Rpsa OE**

148 A decrease in the number of dendrites extending from the soma suggests that defective
149 dendrite initiation has occurred, while a decrease in dendrite length suggests a defect in
150 elongation of dendrites. These early pivotal processes have implications on the remaining stages
151 of neuronal morphogenesis, such as dendritic arborization. *In utero* electroporation was used to
152 induce a CRISPR/Cas9 mediated KD of Rpsa at E15.5 and neuronal morphology was analyzed
153 at P15, since neuritogenesis well-established by this time point. The Rpsa KD neurons had
154 significantly fewer and shorter extensions with less complex branching as compared with the
155 control CRISPR neurons (Fig. 3A). The mean number of dendrites from the soma in Rpsa
156 deficient cells was 2.9 ± 0.24, while the mean number of dendrites, including apical and basal
157 dendrites, from the soma of control neurons was 4.2 ± 0.24 (Fig. 3B). The mean dendrite length
158 in Rpsa deficient cells was 20.9 μm ± 2.0 as compared to control neurons with a mean dendrite
159 length of 49.5 μm ± 2.2 (Fig. 3C). Additionally, Sholl analysis of Rpsa deficient neurons
160 indicates that the Rpsa KD neurons have a severe defect in dendritic branching (Fig. 3D). The
161 Sholl profile is consistent with our analysis of dendrite number and length, since it also indicates
162 that Rpsa deficient cells have fewer and shorter dendrites than controls. All described
163 morphological deficits from Rpsa KD were rescued by CRISPR-resistant Rpsa OE, making it
164 unlikely that the observed phenotype was due to off-target effects (Fig. 3). This suggests that
165 Rpsa signaling is crucial in regulating dendrite formation, during both initiation and elongation,
166 in addition to dendritic arborization. Since the apical dendrite was correctly extended as observed
167 at P3 (Suppl. Fig. 2), the defects in the initiation of dendrites are mainly in basal dendrites.

168 **Rpsa and PEDF show similar defects in neuronal morphology after KD and Rpsa OE can**
169 **rescue morphological defects after PEDF KD**

170 Since PEDF is a known ligand of Rpsa that has neurotrophic properties and is encoded in
171 the clinically relevant Miller-Dieker Syndrome critical region of chromosome 17p13.3, we
172 investigated whether PEDF binding was responsible for initiating Rpsa signaling to regulate
173 neuronal morphogenesis. We used PEDF shRNA in combination with *in utero* electroporation to
174 conduct an initial analysis of PEDF deficient neurons *in vivo*. KD efficiency of the PEDF shRNA
175 was tested via Western Blot and the knockdown efficiency was approximately 84% (Suppl. Fig.
176 1A and B). The initial analysis revealed that PEDF deficient neurons showed similar defects to
177 Rpsa deficient neurons in morphogenesis, with PEDF KD neurons having significantly fewer
178 and shorter extensions with less complex branching as compared with the scramble shRNA
179 control neurons (Fig. 4A). The mean number of dendrites from the soma in PEDF deficient cells
180 was 2.6 ± 0.21, while the mean number of dendrites from the soma in control neurons was 4.4 ±
181 0.25 (Fig. 4B). The mean dendrite length in PEDF deficient cells was 27.0 μm ± 2.6 as compared
182 to control neurons with a mean dendrite length of 50.9 μm ± 3.6 (Fig. 4C). These data indicate
183 that PEDF is important for the initiation and elongation of dendrites. Additionally, Sholl analysis
184 of PEDF deficient neurons indicates that these neurons have a severe defect in dendritic
185 branching (Fig. 4D). The Sholl profile is consistent with our analysis of dendrite number and
186 length, since it also indicates that PEDF deficient cells have fewer and shorter dendrites than
187 controls.

188 To determine whether these similar phenotypes could be a result of PEDF and Rpsa
189 functioning in the same signaling pathway we overexpressed Rpsa in PEDF deficient cells. Rpsa
190 OE rescued morphological defects in the initiation and elongation of dendrites after PEDF KD *in*

191 *vivo* (Fig. 4A). The mean number of dendrites from the soma in PEDF KD + Rpsa OE neurons
192 was 4.2 ± 0.17, which was not significantly different from the mean of 4.35 ± 0.30 for the double
193 transfected control neurons (scramble shRNA + control OE) (Fig. 4B). The mean dendrite length
194 in PEDF KD + Rpsa OE neurons was 44.3 μm ± 3.6, which was not significantly different from
195 the double transfected control neurons (scramble shRNA + control OE) with a mean dendrite
196 length of 44.3 μm ± 3.3 (Fig. 4C). These data indicate that PEDF is involved in Rpsa-mediated
197 initiation and elongation of dendrites. Additionally, Sholl analysis of PEDF KD + Rpsa OE
198 neurons indicates that the branching complexity is similar to that of the double transfected
199 control neurons (Fig. 4D). Taken together with the fact that PEDF is a ligand of Rpsa, these
200 results suggest that PEDF binding initiates Rpsa signaling to regulate neuronal morphogenesis.

201 **Rpsa and Itga6 show similar defects in neuronal morphology after KD and Itga6 OE can**
202 **rescue morphological defects after PEDF KD and increase Rpsa expression on the plasma**
203 **membrane**

204 Rpsa is known to bind to Itga6 on the plasma membrane (25). To determine if Itga6 is
205 also involved in PEDF-Rpsa signaling, we used Itga6 shRNA in combination with *in utero*
206 electroporation at E15.5 to conduct an initial analysis of Itga6 deficient neurons *in vivo*. KD
207 efficiency of the Itga6 shRNA was tested via Western Blot and the knockdown efficiency was
208 approximately 79% (Suppl. Fig. 1A and B). The analysis revealed that Itga6 deficient neurons
209 showed similar defects to Rpsa and PEDF deficient neurons in neuronal morphogenesis (Fig.
210 4A). The mean number of dendrites from the soma in Itga6 deficient cells was 2.5 ± 0.24, while
211 the mean number of dendrites from the soma in control neurons was 4.4 ± 0.25 (Fig. 4B). The
212 mean dendrite length in Itga6 deficient cells was 34.3 μm ± 2.7 as compared to control neurons
213 with a mean dendrite length of 50.9 μm ± 3.6 (Fig. 4C). These data indicate that Itga6 is a key

214 protein for the initiation and elongation of dendrites. Additionally, Sholl analysis of Itga6
215 deficient neurons indicates that these neurons have a severe defect in dendritic branching as seen
216 in neurons deficient in Rpsa and PEDF (Fig. 4D).

217 To determine whether Itga6 is involved in PEDF signaling, we overexpressed Itga6 in
218 PEDF deficient cells. We found that Itga6 OE in PEDF deficient neurons can rescue the
219 morphological defects associated with PEDF KD (Fig. 4A). This rescue phenotype was similar
220 to the control (scramble shRNA + control OE) and PEDF shRNA + Rpsa OE phenotypes. Thus,
221 these results suggest that Itga6 is involved in signaling pathway involving PEDF and Rpsa. The
222 mean number of dendrites from the soma in PEDF KD + Itga6 OE neurons was 4.1 ± 0.29,
223 which was not significantly different from the mean of 4.35 ± 0.30 for the double transfected
224 control neurons (scramble shRNA + control OE) (Fig. 4B). The mean dendrite length in PEDF
225 KD + Itga6 OE neurons was 44.8 μm ± 3.4, which was not significantly different from the
226 double transfected control neurons (scramble shRNA + control OE) with a mean dendrite length
227 of 44.3 μm ± 3.3 (Fig. 4C). This indicates that Itga6 is involved both in the initiation and
228 elongation of dendrites mediated by PEDF and Rpsa. Additionally, Sholl analysis of PEDF KD +
229 Itga6 OE neurons indicates that the branching complexity is partially restored (Fig. 4D). These
230 results suggest that Itga6, a known binding partner of Rpsa, is important for PEDF-Rpsa
231 signaling to regulate dendrite formation during initiation and elongation stages, and possibly
232 dendritic branching.

233 Rpsa and Itga6 expression have been shown to be co-regulated and Rpsa and Itga6 co-
234 localize in the cytosol, possibly leading to their being trafficked together to the plasma
235 membrane (24, 25). We tested whether Itga6 could be increasing Rpsa expression on the plasma
236 membrane, which would allow PEDF-Rpsa signaling to occur more efficiently. We transfected

237 6XHis-Rpsa (only Rpsa OE) and 6XHis-Rpsa + FLAG-Itga6 (both Rpsa and Itga6 OE) into
238 COS-1 cells and performed subcellular fraction to isolate the nuclear, cytoplasmic, and
239 membrane fractions. Then, Rpsa expression level in the 6XHis-Rpsa + FLAG-Itga6 group was
240 analyzed and compared to the control OE group and Rpsa OE only group. We found that Rpsa
241 expression on the plasma membrane was increased with Itga6 OE, as compared to when only
242 Rpsa was overexpressed (Fig. 4E). This suggests that Itga6 could be contributing to PEDF-Rpsa
243 signaling to regulate neuronal morphology by increasing the amount of Rpsa available on the
244 plasma membrane to participate in signaling and may explain the similar neuronal morphology
245 phenotypes following Rpsa KD, PEDF KD, and Itga6 KD.

246 **Rpsa KD and PEDF KD, but not Itga6 KD, cause a decrease in overall spine density and a**
247 **change in spine morphology**

248 We further investigated the neuromorphological changes observed after Rpsa KD, PEDF
249 KD, and Itga6 KD by determining if there was a change in dendritic spine density and
250 morphology, since these factors can impact synaptic function. We used *in utero* electroporation
251 at E15.5 to transfect the relevant plasmids and analyzed spines at P15 (Fig. 5A). We observed a
252 decrease in overall spine density after Rpsa KD (0.28 ± 0.04) and PEDF KD (0.21 ± .04), as
253 compared to the control CRISPR (0.70 ± 0.05) and scramble shRNA (0.97 ± 0.09) controls,
254 respectively (Fig. 5B). Although fewer spines were observed, there was an increase in spines
255 with more immature morphologies such as filopodia and thin in the Rpsa KD and PEDF KD
256 groups (Fig. 5C). Interestingly, Itga6 KD (1.01 ± 0.10) resulted in a spine density phenotype
257 similar to that of the scramble shRNA control group (Fig. 5B). The Itga6 KD and scramble
258 shRNA groups also showed similar spine morphology phenotypes, with most spines being
259 characterized as mushroom (Fig. 5C).

260 To determine whether Rpsa OE could rescue spine defects after PEDF KD, we used *in*
261 *utero* electroporation at E15.5 to overexpress Rpsa in PEDF deficient cells (Fig. 5A). The PEDF
262 shRNA + Rpsa OE group (0.99 ± 0.07) showed an overall spine density that was comparable to
263 the scramble shRNA + control OE group (0.77 ± 0.08) (Fig. 5B). The morphological defects
264 were also rescued, with the PEDF shRNA + Rpsa OE and scramble shRNA + control OE groups
265 having mostly mushroom spines (Fig. 5C). This suggests that PEDF-Rpsa signaling regulates
266 spine density and morphology, while Itga6 may specifically regulate formation of dendrites.

267 **Calcium imaging of brain slices shows sub-threshold functional difference in Rpsa KD**
268 **neurons**

269 We next investigated whether the Rpsa KD associated decrease in dendrite number and
270 length, as well as reduced dendritic arborization and change in spine density and morphology
271 could be linked to functional deficits, since neuronal morphology is a critical factor in
272 determining the extent of inputs received by the neuron. To investigate function in Rpsa deficient
273 neurons we conducted calcium imaging using live brain slices after *in utero* electroporation at
274 E15.5 collected from mice (P15-P60). The calcium indicator GCaMP6s was used to image
275 neurons double-positive for Rpsa or control CRISPR (tdTomato) and GCaMP6s (GFP).
276 GCaMP6s has a relatively high sensitivity and is a well-validated calcium indicator (29). Rpsa
277 deficient neurons had a significantly lower mean difference between maximum and minimum
278 peaks (6.7 ±1.8), as compared with control neurons (12.8 ± 1.1) when spontaneous calcium
279 activity was measured (Fig. 6A), indicating that the Rpsa deficient neurons show significantly
280 decreased calcium signaling. We found that Rpsa KD neurons showed almost no fluctuation in
281 fluorescence intensity, while the control CRISPR neurons showed a dramatically greater change
282 in fluorescence intensity (Fig. 6B). Since few action potentials were recorded, these differences

283 in fluorescence intensity indicate that Rpsa KD neurons have a defect in calcium signaling at a
284 sub-threshold level. Calcium signaling directly relates to neuronal function by contributing to
285 transmission of the depolarizing signal, synaptic signaling processes, neuronal energy
286 metabolism, and neurotransmission (30).

287 To complement our calcium imaging data, we conducted whole-cell electrophysiological
288 recordings in mice (P15-P60) after knocking down Rpsa by CRISPR by *in utero* electroporation
289 at E15.5. In agreement with our calcium imaging results, electrophysiological recordings showed
290 that control and Rpsa KD neurons do not fire action potentials spontaneously at rest (Fig. 6C).
291 However, both control and Rpsa deficient neurons fired action potentials upon stimulation
292 (Suppl. Fig. 3). Intrinsic membrane properties were comparable between groups and only
293 differed significantly in capacitance, indicating a difference in cell size (Suppl. Fig. 3 and Table
294 1). Taken together, this corroborates our calcium imaging results by confirming the low
295 spontaneous firing rate in both control and Rpsa KD cells and showing that Rpsa KD neurons are
296 healthy and able to fire action potentials.

Table 1. Comparison of membrane properties between Control CRISPR and Rpsa CRISPR

	Vm (mV)	Resistance (MΩ)	τ (ms)	C (pF)	Rheobase (pA)	Spike height (mV)	Overshoot (mV)	Spike threshold (mV)
Control CRISPR (n=9)	-67 ± 1.2	60 ± 4.9	14 ± 1.2	251 ± 30.2	141 ± 10.5	84 ± 1.8	50 ± 1.2	-34 ± 1.1
Rpsa CRISPR (n=7)	-64 ± 0.9	50 ± 5.1	18 ± 2.6	369 ± 35.8	149 ± 33.3	81 ± 1.7	48 ± 2.4	-32 ± 1.2

297 Vm = membrane potential, τ = membrane time constant, C = capacitance
298 Data are represented as mean ± SEM.

Discussion

Our study reports a role for Rpsa in regulating neuronal morphogenesis, including dendrite formation, apical dendrite orientation, dendritic branching, and spine density and morphology and suggests that morphological defects caused by Rpsa KD have sub-threshold functional consequences for calcium signaling. By performing *in vivo* rescue experiments, we found that PEDF-Rpsa-Itga6 signaling is essential for neuromorphogenesis.

Orientation of the apical dendrite and neuronal morphogenesis was dramatically impacted by disrupting Rpsa signaling. Improper orientation of the apical dendrite may have led to formation of inappropriate synaptic connections, since the apical dendrite may not have been within sufficient vicinity of its target neuron to allow synaptogenesis to occur. The decrease in number of dendrites and dendrite length suggests a deficit in the initiation and elongation of dendrites, respectively. Defects in these early stages of morphogenesis may have caused further defects at later stages such as dendritic arborization, as a severe defect in dendritic branching was observed in Rpsa deficient neurons. Rpsa deficient neurons show aberrant orientation of the apical dendrite at the proximal region of the apical dendrites (Fig. 2). However, the distal region of apical dendrites turns into the proper direction to the marginal zone (Fig. 2A). This implies that Rpsa affects the very initial step of dendrite extension after its initiation from soma, but not the later dendrite extension step. Future studies including time-lapse live imaging will help understand the precise function of Rpsa in regulating dendrite behavior during the initial step of dendrite extension and orientation.

While a significant decrease in dendrite length was seen at P15 (Fig. 3), no difference was observed between Rpsa KD and control CRISPR in dendrite length at P3 (Suppl. Fig. 2). The mean length measurement at P3 is heavily influenced by the length of the apical dendrite

322 since it is one of the only extensions present at this developmental time-point and basal dendrites
323 were not yet formed. Therefore, the defects in dendrite length seen at P15 resulted from the
324 defects in basal dendrites, indicating the importance of Rpsa in basal dendrite formation.
325 Genetically manipulating the proposed Rpsa signaling pathway using various rescue
326 experiments allowed us to provide convincing evidence that PEDF is the ligand responsible for
327 initiating Rpsa signaling to regulate neuronal morphogenesis and that an Rpsa-Itga6 signaling
328 complex is important for this pathway (Fig. 7A). Since the ligand PEDF is upstream of its
329 receptor Rpsa, Rpsa OE should compensate for a decrease in PEDF. Some PEDF will still be
330 present, since the knockdown does not lead to complete loss of PEDF and the cells not
331 transfected by *in utero* electroporation will still normally secrete PEDF. Thus, Rpsa OE should
332 increase the opportunity for the PEDF that is present to bind to an Rpsa receptor and compensate
333 for the PEDF KD. Since Itga6 OE had a similar result as Rpsa OE, this suggests that an increase
334 in Itga6 expression may lead to an increase in Rpsa localization on the plasma membrane,
335 producing a similar effect to Rpsa OE. Therefore, the PEDF-Rpsa signaling may regulate
336 several aspects of neuronal morphogenesis including dendrite initiation, dendrite elongation,
337 dendritic branching, and spine formation (Fig. 7A). The overexpression of Rpsa and Itga6 in
338 combination with cellular fractionation revealed that Itga6 OE facilitates Rpsa expression on the
339 plasma membrane (Fig. 4E). A potential mechanistic explanation is that Rpsa and Itga6 bind
340 each other in the cytoplasm and Itga6 supports the expression of Rpsa on the plasma membrane
341 (Fig. 7B). Another possible model is that Rpsa and Itga6 independently express on the plasma
342 membrane and Itga6 stabilizes the expression of Rpsa (Fig. 7B). Further research should be done
343 to investigate the molecular mechanisms that drive relationship between Rpsa and Itga6 in more
344 detail. While Itag6 has an important role in PEDF-Rpsa signaling, Itga6 regulation during

345 neuronal morphogenesis appears to be specific to dendrite formation. Interestingly, Itga6 does
346 not seem to have a role in regulating dendritic spine density or dendritic spine morphology, and
347 may only have a limited role in regulation of dendritic branching.

348 The Sholl profiles for both the PEDF shRNA + Rpsa OE and PEDF shRNA + Itga6 OE
349 rescue experiments show an increase in complexity of dendritic branching as compared to the
350 PEDF shRNA group, indicating that overexpression of either Rpsa or Itga6 rescues this aspect of
351 the PEDF KD phenotype to some extent (Fig. 4D). However, the PEDF shRNA + Rpsa OE
352 group showed even more complex branching than the scramble shRNA + control OE group,
353 while the PEDF shRNA + Itga6 OE showed a less complex branching phenotype as compared to
354 the scramble shRNA + control OE group. Rpsa OE could have resulted in a more complex
355 branching phenotype, since Rpsa is further downstream than PEDF in the proposed signaling
356 pathway. Thus, overexpression at a more downstream level in the signaling pathway could have
357 overstimulated the mechanism responsible for regulating branching, leading to an increase in
358 branching complexity.

359 To determine whether the dramatic morphological defects caused by Rpsa KD impact
360 function, we conducted calcium imaging on live brain slices and detected a difference between
361 Rpsa KD cells and control cells in sub-threshold calcium signaling. The GCaMP6s calcium
362 indicator was used, which has a relatively high sensitivity and has commonly been used to image
363 relatively low cytoplasmic calcium levels (29). The percent change in fluorescence fluctuates for
364 the control, while Rpsa deficient cells appear to maintain a constant level of fluorescence even
365 when the recording period was substantially extended. Sub-threshold changes in calcium
366 signaling in Rpsa KD neurons could be due to differences in NMDA channel, NMDA receptor
367 (NMDAR), or voltage-gated calcium channels (VGCCs) functions, which could be reduced

368 simply because of the decrease in dendritic surface area by less dendrites and shorter dendrite
369 length (31-35). Many previous studies differ from ours in that they focus on calcium signaling in
370 active spines. However, the amount of calcium that enters via these synaptic mechanisms may be
371 very small, requiring that the signal be greatly amplified by intracellular calcium release to be
372 detected (36). We would be able to detect sub-threshold calcium signaling changes resulting
373 from calcium release from internal stores in the soma. The morphological defects caused by
374 Rpsa KD may be impacting the NMDA, NMDAR, and/or VGCCs responsible for mediating
375 calcium influx, thus resulting in sub-threshold calcium signaling changes.

376 Single action potentials are defined as $\Delta F/F_0 \geq 23\% \pm 3.2\%$. Thus, few action potentials
377 were recorded by our calcium imaging. However, this is not surprising, since pyramidal cells can
378 have a low spontaneous firing rate (37). Our electrophysiology recordings confirm the minimal
379 percent change in fluorescence detected by our calcium imaging by showing that inputs do not
380 summate to a level that would cause action potentials for either the Rpsa KD or control group.
381 This indicates that the specific cortical pyramidal neurons that were transfected via *in utero*
382 electroporation have a low spontaneous firing rate. Thus, we should not expect to see many
383 action potentials recorded in our calcium imaging experiments. Taken together, these data
384 suggest that Rpsa KD causes a functional difference in calcium signaling at sub-threshold levels
385 in cortical pyramidal neurons with a low spontaneous firing rate.

386 Additionally, our electrophysiology recordings indicate that control CRISPR neurons and
387 Rpsa CRISPR neurons display similar intrinsic membrane properties (Suppl. Fig. 3 and Table 1).
388 This is important to note because the 37-kDa Rpsa precursor is a component of the 40S ribosome
389 and is involved in pre-RNA processing, thus it could be suggested that the morphological defects
390 in Rpsa deficient cells may be attributed to a poor overall state of the neurons (5, 38). However,

391 our electrophysiology results suggest that Rpsa deficient cells remain healthy, despite the
392 phenotypic changes associated with Rpsa KD (Suppl. Fig. 3 and Table 1). Furthermore, we show
393 that Itga6 enhances Rpsa's expression on the membrane, where it must be located to interact with
394 its extracellular ligand PEDF, indicating that Rpsa's role as a receptor is critical for regulating
395 neuromorphogenesis.

396 These results are of clinical interest because the *Serpinf1* gene, coding for PEDF protein,
397 is located in the chromosome 17p13.3 region, which is often deleted causing Miller-Dieker
398 Syndrome (MDS) and duplicated causing the 17p13.3 microduplication syndrome. There is no
399 doubt that neuronal migration defects are a main cause of MDS, but the pathogenesis of MDS
400 has not been completely clarified in detail. MDS has a complex etiology because it caused by a
401 microdeletion that could include more than 26 genes, including *Serpinf1*. While most of the
402 genes deleted in MDS patients have not been investigated, previous studies have analyzed some
403 genes, including *Pafah1b1* (Lis1), *Ywhae* (14-3-3ε) and *Crk* in the MDS critical region (22, 39-
404 43). However, these studies focused on the gene functions in neuronal migration and neural
405 activity, since most MDS patients suffer from epilepsy. The role of neuronal morphogenesis in
406 MDS etiology remains uncertain. PEDF deficiency may not be the main cause of MDS, but it
407 could contribute to MDS pathogenesis. Thus, our findings will provide new insights into the
408 mechanisms underlying MDS.

409 In conclusion, Rpsa signaling mediates functionally relevant aspects of cortical neuronal
410 morphogenesis including apical dendrite orientation, initiation and elongation of dendrites,
411 dendritic branching, and dendritic spine density and morphology. This Rpsa signaling
412 mechanism is initiated by binding of its ligand PEDF, while Rpsa transduces the PEDF-initiated
413 signal via Itga6. Future studies should focus on elucidating the downstream targets of Rpsa

414 during cortical neuronal morphogenesis and investigating the mechanism by which Rpsa KD
415 impacts the synapse. Further investigation can advance our understanding of neuronal
416 morphogenesis in normal brain development as well as increase our knowledge of
417 neurodevelopmental disorders, such as MDS.

418 **Materials and Methods**

419 **Mice**

420 All animal experiments were performed under protocols approved by the Drexel
421 University Animal Care and Use Committees and following the guidelines provided by the US
422 National Institutes of Health. ICR mice were purchased from Taconic Inc. Embryonic day (E)
423 0.5 was defined as noon of the day the vaginal plug appeared.

424 **Plasmids**

425 pCAG-eCas9-GFP-U6-gRNA was a gift from Jizhong Zou (Addgene plasmid # 79145 ;
426 http://n2t.net/addgene:79145 ; RRID:Addgene_79145). This plasmid contains high-fidelity
427 eSpCas9 to reduce the off-target effects. gRNAs were designed using the web-based design
428 tools, including CHOPCHOP (http://chopchop.cbu.uib.no/) and CRISPy-web
429 (https://crispy.secondarymetabolites.org/#/input), and then cloned into pCAG-eCas9-GFP-U6-
430 gRNA. Rpsa target gRNA sequence is ATCTACAAAAGGAAAAGTGA(CGG) (112-131 of
431 mouse Rpsa). CRISPR was chosen as the method to accomplish Rpsa KD, as opposed to shRNA,
432 because we were not able to identify a specific shRNA target sequence using web-based design
433 tools (InvivoGen siRNA Wizard, and Invitrogen Block-iT RNAi Designer). For calcium
434 imaging, GFP in pCAG-eCas9-GFP-U6-control-gRNA and pCAG-eCas9-GFP-U6-Rpsa-gRNA
435 was replaced into tdTomato by PCR. 6XHis-tagged Rpsa was cloned into pCAGItdTomato
436 vector (pCAGItdTomato-Rpsa) as described previously (44). CRISPR-resistant Rpsa
437 overexpression plasmid was created by PCR. The sense and antisense primers containing the
438 CRISPR target sequence with mutations were designed, and PCR was performed using
439 PrimeSTAR GXL (Takara) with pCAGItdTomato-Rpsa. Ten mutations without amino acid
440 change were introduced into primers. The sequence with mutation is

441 ATTTATAAGCGCAAGTCAGA(TGG) where underlined nucleotides are mutated. The
442 insertion of mutations was confirmed by sequencing. To create pCAGEN-GCaMP6s, pCAGEN
443 and pGP-CMV-GCaMP6s were obtained from Addgene, and GCaMP6s fragment amplified by
444 PCR was cloned into pCAGEN. pGP-CMV-GCaMP6s was a gift from Douglas Kim (Addgene
445 plasmid # 40753 ; http://n2t.net/addgene:40753 ; RRID:Addgene_40753)(29). pCAGEN was a
446 gift from Connie Cepko (Addgene plasmid # 11160 ; http://n2t.net/addgene:11160 ;
447 RRID:Addgene_11160) (45). PEDF and Itga6 shRNAs were designed using the web-based tools
448 described above and cloned into pSCV2-Venus plasmid as described previously (44, 46). The
449 target sequence of mouse PEDF is GAACTTGACCATGATAGAA (849-867). The target
450 sequence for mouse Itga6 shRNA is GACCAAAGACTCGATGTTT (1113-1131). Certified
451 scramble shRNA (ACTACCGTTGTTATAGGTG) was also used as a negative control
452 (Invitrogen). All plasmids used in this study were purified by NucleoBond Xtra purification kit
453 (MACHEREY-NAGEL). pLenti-CMV-Itga6-Myc-DDK-P2A-Puro vector was purchased from
454 Origene Technologies, Inc. (PS100092). Itga6-Myc-DDk fragment was amplified by PCR and
455 cloned into pLV-CAG-P2A-mScarlet plasmid.

456 **Analysis of genomic alterations by CRISPR/Cas9**

457 pCAG-eCas9-GFP-U6-Rpsa-gRNA plasmid was transfected into mouse Neuro-2a cells
458 using PolyJet transfection reagent (SignaGen Laboratories), and Genomic DNA was isolated and
459 subjected to PCR to amplify the 433 bp fragment containing gRNA target sequence using Q5
460 High Fidelity DNA polymerase (NEB) and primers
461 (GAATTC(EcoRI)/GAGTTCTAGTGTCAGAAGAAAAAAGATGAATTTTATTCC and
462 GGATCC(BamHI)/AGCTTTAATAGTGTGCAGGGTCAGTCAG). PCR products were

463 purified by PCR clean-up/Gel extraction kit (MACHEREY-NAGEL) and cloned into
464 pBluescript SK(+). Plasmid DNA isolated from the transformed bacteria was sequenced.

465 **Antibodies**

466 The primary and secondary antibodies used in this research were as follows: Anti-Rpsa
467 (Santa Cruz, sc-376295), Anti-GAPDH (Proteintech, 60004-1-Ig), Anti-PEDF (Santa Cruz, sc-
468 16956), Anti-His-Tag (Proteintech, 66005-1-Ig), Anti-βIII tubulin (Thermo Scientific Pierce,
469 2G10), Anti- DYKDDDDK epitope (FLAG) tag (Thermo Scientific Pierce, MA1-91878).

470 **Histology and Immunohistochemistry**

471 To analyze Rpsa expression, brains were dissected at E18.5 and fixed with
472 paraformaldehyde/Phosphate-buffered saline overnight at 4°C. Fixed samples were cryo-
473 protected by 25% sucrose/Phosphate-buffered saline for 48 hours at 4°C and then embedded with
474 O.C.T. compound (Sakura). Cryo-sections (30 μm thickness) were cut by cryostat (Microm
475 HM505 N) and air dried. Sections were rinsed three times in Tris-buffered saline and treated
476 with 0.2% Triton X-100/Tris-buffered saline for 10 minutes at room temperature, followed by
477 blocking for 30 minutes in 5% Bovine serum albumin/Phosphate-buffered saline supplemented
478 with 0.25% Tween-20 to prevent nonspecific binding. Primary antibodies were diluted in
479 blocking buffer, and sections were incubated in primary antibody overnight at 4°C. All
480 secondary antibodies were diluted with blocking buffer and sections were incubated in secondary
481 antibody for 30 minutes at room temperature. Sections were stained by 40,6-Diamidino-2-
482 phenylindole, Dihydrochloride (DAPI, 600nM) and embedded with 90% glycerol made with
483 Tris-buffered saline.

484 To analyze neuronal morphology, brains were dissected at postnatal day (P) 3 or P15 and
485 fixed with paraformaldehyde/Phosphate-buffered saline overnight at 4°C. Fixed samples were
486 processed as described above. Cryo-sections (60 µm thickness) were cut and stained by DAPI.

487 ***In Utero* Electroporation**

488 *In utero* electroporation was performed as previously described (40, 44, 47). Briefly,
489 pregnant dams were anesthetized with Avatin and the uterine horn was exposed. Plasmids (1 µg)
490 were then injected into the lateral ventricle of E15.5 embryo brains. Electroporation at E15.5 will
491 allow for transfection of cortical pyramidal neurons in layer 2/3 (26-28). Embryo heads were
492 placed between electrodes with the positive anode angled toward the cortex and three electric
493 pulses of 35 mV were applied with 50 ms intervals by a CUY21 electroporator (Nepa GENE).
494 Embryos were placed back into the uterus and allowed to develop uninterrupted until brain
495 samples were collected at P3 or P15.

496 **Analysis of Neuronal Morphology**

497 All images were obtained using a confocal microscope (Leica SP8) and the experimenter
498 was blind to the phenotype at the time of imaging.

499 Apical Dendrite Orientation at P3 – The angle at which the apical dendrite extends with
500 respect to the cortical plate at P3 was measured using the ImageJ software angle tool. A straight
501 line perpendicular to the edge of the tissue was used as a reference point to start measuring the
502 angle. Absolute values of the measured angles were used to calculate mean angles. Standard
503 deviation projection images from z-projection photos produced from z-stack data were used for
504 analysis.

505 Neuronal Morphology Analysis at P15 – ImageJ software measuring features were used
506 to analyze neuronal morphology. Standard deviation projection images from z-projection photos

507 produced from z-stack data were used for analysis. Sholl analysis was performed using the Sholl
508 Analysis Plugin (Gosh Lab, UCSD) for ImageJ following the developer instructions.
509 Dendritic Spine Morphology Analysis at P15 – Spines were objectively characterized
510 based on geometric characteristics. Spines longer than 1 μm were classified as filopodia, while
511 spines shorter than 1 μm were classified as thin. Stubby and mushroom spines were classified
512 based on morphological appearance. Spines with two heads were classified as branched. Photos
513 of spines were taken at 63x with 5x zoom and standard deviation projection images were used
514 for analysis.

515 **Subcellular Fractionation**

516 The subcellular fractionation kit (NBP2-47659) from Novus Biologicals was used to fractionate
517 COS-1 cells according to the protocol provided by the manufacturer.

518 **Calcium Imaging of Live Brain Slices**

519 Slice Preparation – Brain slices were prepared using a modified version of a previously
520 described protocol (44). Briefly, mice (P15-P60) were decapitated and brains were quickly
521 removed and placed in ice cold high sucrose artificial cerebral spinal fluid (ACSF) solution for
522 slicing. Brains were embedded in 4% low-melting agarose and coronal cortical slices were
523 generated (300 μm) with a vibrating microtome (VTS1000 Leica Microsystems). Slices were
524 next incubated for 60 minutes at 37°C in DMEM/F-12 imaging media without phenol red
525 supplemented with 10% fetal bovine serum (FBS).
526 Imaging of Spontaneous Activity – The experimenter was blind to the phenotype at the
527 time of the imaging. Slices were gently transferred into glass bottom 35mm dishes (MatTek) for
528 imaging. A membrane was placed on top of the slices to reduce movement during imaging.
529 Time-lapse live imaging was performed using an inverted fluorescent microscope (Ziess, Axio

530 Observer Z1) with a 20x objective. Images were captured every 50 ms for 1 minute while the
531 slices were maintained at 37°C with a stage top incubator (Zeiss).

532 Calcium Imaging Data Analysis – All cells included in the analysis were double-positive
533 for GCamp6s and either pCAG-eCas9-tdTomato-U6-control-gRNA or pCAG-eCas9-tdTomato-
534 U6-Rpsa-gRNA. All image analysis was performed using Zen 2 Pro analysis software (Ziess
535 2011). Circular regions of interest were placed on the cell soma. Baseline fluorescence (F_0) was
536 obtained by averaging the fluorescence intensity inside the region of interest immediately before
537 beginning the time course imaging. Images were captured every 50ms for 1 minute.
538 Fluorescence intensity for the time course was measured by averaging all pixels in the region of
539 interest at each frame of the imaging (29). Percent change in fluorescence ($\Delta F/F_0$) was calculated
540 as ($F_{measured}$- F_0)/ F_0 for every frame of the time course.

541 **Electrophysiological Recordings**

542 Slice Preparation – Mice (P15-P60) were decapitated and brains were quickly removed
543 and placed in ice cold sucrose solution containing the following (in mM): 87 NaCl, 75 sucrose,
544 25 glucose, 25 $NaHCO_3$, 1.25 NaH_2PO_4, 2.5 KCl, 0.25 $CaCl_2$, and 3.5 $MgSO_4$ for slicing.
545 Coronal cortical slices were generated (300 μm) with a vibrating microtome (Leica
546 Microsystems). Slices were next incubated for 30 minutes at 37°C in recording artificial
547 cerebrospinal fluid (ACSF) containing the following (in mM): 111 NaCl, 3 KCl, 11 glucose, 25
548 $NaHCO_3$, 1.3 $MgSO_4$, 1.1 KH_2PO_4, and 2.5 $CaCl_2$. Slices were then maintained at room-
549 temperature in ACSF for at least 30 minutes before recording. Both slicing solutions and
550 recording solutions were continuously aerated with 95%/5% CO_2/O_2.

551 Recordings – The experimenter was blind to the phenotype at the time of the recording.
552 All recordings were performed at room temperature. Cortical neurons transfected with either the

553 control CRISPR plasmid or the Rpsa CRISPR plasmid were visualized based on their
554 fluorescence (tdTomato) with a 63x objective lens on a BX51WI scope (Olympus) using LED
555 illumination (X-cite). Patch electrodes (Harvard Apparatus) were pulled to tip resistances of 5-8
556 MΩ using a multi-stage puller (Sutter Instruments) and were filled with K-gluconate based
557 intracellular solution, containing the following (in mM): 128 K-gluconate, 10 HEPES, 0.0001
558 $CaCl_2$, 1 glucose, 4 NaCl, 5 ATP, and 0.3 GTP. Data was collected with a Multiclamp 700B
559 amplifier (Molecular Devices) and Clampex software (pClamp9, Molecular Devices). Signals
560 were digitized at 20 kHz and filtered at 4 kHz.

561 Resting membrane potential of the neuron was recorded in current-clamp mode
562 immediately after breaking in. For passive and active membrane properties, current- and voltage-
563 clamp protocols were performed as previously described(29). Briefly, input resistance was
564 measured from a series of hyperpolarizing steps in voltage clamp using Clampfit. Time constant,
565 tau, was calculated from the standard exponential fit of hyperpolarizing steps in current clamp.
566 Capacitance was calculated from the input resistance and the tau measurements. Rheobase was
567 defined as the lowest current step (in 10 pA increments) that evoked an action potential in the
568 neuron.

569 **Statistical Analysis**

570 Quantitative data were subjected to statistical analysis using SPSS (IBM Analytics) and
571 MATLAB (MathWorks). The data were analyzed by two-tailed independent-samples t-tests or
572 one-way ANOVAs when appropriate. Values represented as mean ± S.E.M. Results were
573 deemed statistically significant if the p value was <0.05.

Acknowledgements

We thank Dr. Bryan W. Luikart for his technical advice and support. We are also grateful to Drs. Peter Baas, Elias Spiliotis, Eric Olson, and Itzhak Fischer for their reading the manuscript and comments.

Financial Disclosure

This work has been supported by a research grant from the NINDS (NS096098). The funders had no role in study design, data collection and analysis, decision to publish, or preparation of the manuscript.

Competing Interests

The authors have declared that no competing interests exist.

586 **References**

587 1. Ammar MR, Humeau Y, Hanauer A, Nieswandt B, Bader MF, Vitale N. The Coffin-
588 Lowry syndrome-associated protein RSK2 regulates neurite outgrowth through phosphorylation
589 of phospholipase D1 (PLD1) and synthesis of phosphatidic acid. The Journal of neuroscience :
590 the official journal of the Society for Neuroscience. 2013;33(50):19470-9.

591 2. Wang Q, Moore MJ, Adelmant G, Marto JA, Silver PA. PQBP1, a factor linked to
592 intellectual disability, affects alternative splicing associated with neurite outgrowth. Genes &
593 development. 2013;27(6):615-26.

594 3. Van Maldergem L, Hou Q, Kalscheuer VM, Rio M, Doco-Fenzy M, Medeira A, et al.
595 Loss of function of KIAA2022 causes mild to severe intellectual disability with an autism
596 spectrum disorder and impairs neurite outgrowth. Human molecular genetics. 2013;22(16):3306-
597 14.

598 4. Parrish JZ, Emoto K, Kim MD, Jan YN. Mechanisms that regulate establishment,
599 maintenance, and remodeling of dendritic fields. Annual review of neuroscience. 2007;30:399-
600 423.

601 5. Tohgo A, Takasawa S, Munakata H, Yonekura H, Hayashi N, Okamoto H. Structural
602 determination and characterization of a 40 kDa protein isolated from rat 40 S ribosomal subunit.
603 FEBS Letters. 1994;340(1):133-8.

604 6. Hoshiba Y, Toda T, Ebisu H, Wakimoto M, Yanagi S, Kawasaki H. Sox11 Balances
605 Dendritic Morphogenesis with Neuronal Migration in the Developing Cerebral Cortex. The
606 Journal of Neuroscience. 2016;36(21):5775.

607 7. Häusser M, Spruston N, Stuart GJ. Diversity and Dynamics of Dendritic Signaling.
608 Science. 2000;290(5492):739.

609 8. Ye H, Ling Jessie Tan Y, Ponniah S, Takeda Y, Wang S-Q, Schachner M, et al. Neural
610 recognition molecules CHL1 and NB-3 regulate apical dendrite orientation in the neocortex via
611 PTP alpha 2008. 188-200 p.
612 9. Harris KM, Kater SB. Dendritic spines: Cellular specializations imparting both stability
613 and flexibility to synaptic function. Annual review of neuroscience. 1994;17:341-71.
614 10. Nimchinsky EA, Sabatini BL, Svoboda K. Structure and Function of Dendritic Spines.
615 Annual Review of Physiology. 2002;64(1):313-53.
616 11. Fiala JC, Spacek J, Harris KM. Dendritic Spine Pathology: Cause or Consequence of
617 Neurological Disorders? Brain Research Reviews. 2002;39(1):29-54.
618 12. DiGiacomo V, Meruelo D. Looking into laminin receptor: critical discussion regarding
619 the non-integrin 37/67-kDa laminin receptor/RPSA protein. Biological reviews of the Cambridge
620 Philosophical Society. 2016;91(2):288-310.
621 13. Fujimura Y, Yamada K, Tachibana H. A lipid raft-associated 67kDa laminin receptor
622 mediates suppressive effect of epigallocatechin-3-O-gallate on FcepsilonRI expression.
623 Biochemical and biophysical research communications. 2005;336(2):674-81.
624 14. Lesot H, Kühl U, Mark K. Isolation of a laminin-binding protein from muscle cell
625 membranes. The EMBO journal. 1983;2(6):861-5.
626 15. Malinoff HL, Wicha MS. Isolation of a cell surface receptor protein for laminin from
627 murine fibrosarcoma cells. J Cell Biol. 1983;96(5):1475-9.
628 16. Rao NC, Barsky SH, Terranova VP, Liotta LA. Isolation of a tumor cell laminin receptor.
629 Biochemical and biophysical research communications. 1983;111(3):804-8.
630 17. Gopalakrishna R, Gundimeda U, Zhou S, Bui H, Davis A, McNeill T, et al. Laminin-1
631 induces endocytosis of 67KDa laminin receptor and protects Neuroscreen-1 cells against death

632 induced by serum withdrawal. Biochemical and biophysical research communications.
633 2018;495(1):230-7.
634 18. Bernard A, Gao-Li J, Franco C-A, Bouceba T, Huet A, Li Z. Laminin Receptor
635 Involvement in the Anti-angiogenic Activity of Pigment Epithelium-derived Factor. The Journal
636 of Biological Chemistry. 2009;284(16):10480-90.
637 19. Tombran-Tink J, Barnstable CJ. PEDF: a multifaceted neurotrophic factor. Nature
638 Reviews Neuroscience. 2003;4:628.
639 20. Stevens AR, Ahmed U, Vigneswara V, Ahmed Z. Pigment Epithelium-Derived Factor
640 Promotes Axon Regeneration and Functional Recovery After Spinal Cord Injury. Molecular
641 neurobiology. 2019.
642 21. Pignolo RJ, Cristofalo VJ, Rotenberg MO. Senescent WI-38 cells fail to express EPC-1, a
643 gene induced in young cells upon entry into the G0 state. J Biol Chem. 1993;268(12):8949-57.
644 22. Blazejewski SM, Bennison SA, Smith TH, Toyo-oka K. Neurodevelopmental Genetic
645 Diseases Associated With Microdeletions and Microduplications of Chromosome 17p13.3.
646 Frontiers in Genetics. 2018;9(80).
647 23. Shimojima K, Sugiura C, Takahashi H, Ikegami M, Takahashi Y, Ohno K, et al.
648 Genomic copy number variations at 17p13.3 and epileptogenesis. Epilepsy research. 2010;89(2-
649 3):303-9.
650 24. Romanov V, Sobel ME, pinto da Silva P, Menard S, Castronovo V. Cell localization and
651 redistribution of the 67 kD laminin receptor and alpha 6 beta 1 integrin subunits in response to
652 laminin stimulation: an immunogold electron microscopy study. Cell adhesion and
653 communication. 1994;2(3):201-9.

654 25. Ardini E, Tagliabue E, Magnifico A, Buto S, Castronovo V, Colnaghi MI, et al. Co-
655 regulation and physical association of the 67-kDa monomeric laminin receptor and the
656 alpha6beta4 integrin. J Biol Chem. 1997;272(4):2342-5.
657 26. Matsui A, Yoshida AC, Kubota M, Ogawa M, Shimogori T. Mouse in utero
658 electroporation: controlled spatiotemporal gene transfection. J Vis Exp. 2011(54):3024.
659 27. Quiquempoix M, Fayad SL, Boutourlinsky K, Leresche N, Lambert RC, Bessaih T.
660 Layer 2/3 Pyramidal Neurons Control the Gain of Cortical Output. Cell reports.
661 2018;24(11):2799-807.e4.
662 28. Sehara K, Toda T, Iwai L, Wakimoto M, Tanno K, Matsubayashi Y, et al. Whisker-
663 Related Axonal Patterns and Plasticity of Layer 2/3 Neurons in the Mouse Barrel Cortex. The
664 Journal of Neuroscience. 2010;30(8):3082.
665 29. Chen T-W, Wardill TJ, Sun Y, Pulver SR, Renninger SL, Baohan A, et al. Ultra-sensitive
666 fluorescent proteins for imaging neuronal activity. Nature. 2013;499(7458):295-300.
667 30. Brini M, Cali T, Ottolini D, Carafoli E. Neuronal calcium signaling: function and
668 dysfunction. Cellular and molecular life sciences : CMLS. 2014;71(15):2787-814.
669 31. Schiller J, Schiller Y, Clapham DE. NMDA receptors amplify calcium influx into
670 dendritic spines during associative pre- and postsynaptic activation. Nat Neurosci.
671 1998;1(2):114-8.
672 32. Koester HJ, Sakmann B. Calcium dynamics in single spines during coincident pre- and
673 postsynaptic activity depend on relative timing of back-propagating action potentials and
674 subthreshold excitatory postsynaptic potentials. Proceedings of the National Academy of
675 Sciences. 1998;95(16):9596.

676 33. Kovalchuk Y, Eilers J, Lisman J, Konnerth A. NMDA Receptor-Mediated Subthreshold
677 Ca2+ Signals in Spines of Hippocampal Neurons. The Journal of Neuroscience.
678 2000;20(5):1791.
679 34. Yuste R, Majewska A, Cash SS, Denk W. Mechanisms of Calcium Influx into
680 Hippocampal Spines: Heterogeneity among Spines, Coincidence Detection by NMDA
681 Receptors, and Optical Quantal Analysis. The Journal of Neuroscience. 1999;19(6):1976.
682 35. Magee JC, Christofi G, Miyakawa H, Christie B, Lasser-Ross N, Johnston D.
683 Subthreshold synaptic activation of voltage-gated Ca2+ channels mediates a localized Ca2+
684 influx into the dendrites of hippocampal pyramidal neurons. J Neurophysiol. 1995;74(3):1335-
685 42.
686 36. Emptage N, Bliss TV, Fine A. Single synaptic events evoke NMDA receptor-mediated
687 release of calcium from internal stores in hippocampal dendritic spines. Neuron. 1999;22(1):115-
688 24.
689 37. Petersen CC, Crochet S. Synaptic computation and sensory processing in neocortical
690 layer 2/3. Neuron. 2013;78(1):28-48.
691 38. O'Donohue MF, Choesmel V, Faubladier M, Fichant G, Gleizes PE. Functional
692 dichotomy of ribosomal proteins during the synthesis of mammalian 40S ribosomal subunits. J
693 Cell Biol. 2010;190(5):853-66.
694 39. Henry RK, Astbury C, Stratakis CA, Hickey SE. 17p13.3 microduplication including
695 CRK leads to overgrowth and elevated growth factors: A case report. European journal of
696 medical genetics. 2016;59(10):512-6.

697 40. Cornell B, Wachi T, Zhukarev V, Toyo-oka K. Regulation of neuronal morphogenesis by
698 14-3-3epsilon (Ywhae) via the microtubule binding protein, doublecortin. Human molecular
699 genetics. 2016;25(20):4405-18.
700 41. Hyon C, Marlin S, Chantot-Bastaraud S, Mabboux P, Beaujard MP, Al Ageeli E, et al. A
701 new 17p13.3 microduplication including the PAFAH1B1 and YWHAE genes resulting from an
702 unbalanced X;17 translocation. European journal of medical genetics. 2011;54(3):287-91.
703 42. Nagamani SC, Zhang F, Shchelochkov OA, Bi W, Ou Z, Scaglia F, et al. Microdeletions
704 including YWHAE in the Miller-Dieker syndrome region on chromosome 17p13.3 result in
705 facial dysmorphisms, growth restriction, and cognitive impairment. Journal of medical genetics.
706 2009;46(12):825-33.
707 43. Izumi K, Kuratsuji G, Ikeda K, Takahashi T, Kosaki K. Partial deletion of LIS1: a pitfall
708 in molecular diagnosis of Miller-Dieker syndrome. Pediatr Neurol. 2007;36(4):258-60.
709 44. Wachi T, Cornell B, Marshall C, Zhukarev V, Baas PW, Toyo-oka K. Ablation of the 14-
710 3-3gamma Protein Results in Neuronal Migration Delay and Morphological Defects in the
711 Developing Cerebral Cortex. Developmental neurobiology. 2016;76(6):600-14.
712 45. Matsuda T, Cepko CL. Electroporation and RNA interference in the rodent retina in vivo
713 and in vitro. Proc Natl Acad Sci U S A. 2004;101(1):16-22.
714 46. Hand R, Polleux F. Neurogenin2 regulates the initial axon guidance of cortical pyramidal
715 neurons projecting medially to the corpus callosum. Neural Development. 2011;6(1):30.
716 47. Tabata H, Nakajima K. Efficient in utero gene transfer system to the developing mouse
717 brain using electroporation: visualization of neuronal migration in the developing cortex.
718 Neuroscience. 2001;103(4):865-72.

719

720 **Figure Legends**

721 **Figure 1. Expression of Rpsa in the developing cerebral cortex and in primary cortical**
722 **neuronal culture**

723 A) Western blot showing Rpsa expression level in lysates of the cortex at various developmental
724 time-points. B) Quantification of the Western blot showing Rpsa expression levels in the cortex
725 done using ImageJ. Three biological/technical replicates were used (n = 3). Band intensity was
726 quantified and normalized to glyceraldehyde 3-phosphate dehydrogenase (GAPDH). C)
727 Immunofluorescence staining of wild-type brain slices at E18.5 showing the spatial distribution
728 of Rpsa expression (top x20, bottom x63). Scale bars = 50 µm. D) Immunofluorescence staining
729 of cortical primary neurons after 6 days in culture. Staining shows distribution of Rpsa and
730 neurons are double-positive for neuronal marker Tuj1 (βIII tubulin).

731 **Figure 2. Rpsa CRISPR is associated with apical dendrite misorientation at P3 that can be**
732 **rescued by Rpsa OE**

733 A) Neurons transfected via *in utero* electroporation at E15.5, orientation of the apical dendrite
734 measured using the angle at which the apical dendrite extends from the middle of the soma
735 relative to the cortical plate, scale bar = 50 µm B) One-way ANOVA showed a significant
736 difference in mean angle of apical dendrite from soma ($F(3,76) = 22.620$, $p < 0.0005$). Tukey
737 post hoc test showed degree of angle of apical dendrite from middle of soma is significantly
738 greater for the Rpsa CRISPR group (30.4° ± 3.09) compared to control CRISPR (10.7° ± 1.20)
739 ($p < 0.0005$). There was no significant difference between Rpsa CRISPR + Rpsa OE (10.8° ±
740 1.71) and control CRISPR + control OE groups (12.5° ± 1.49) (p=0.924). For all groups n=21
741 cells from 3 mice. Data are represented as mean ± SEM. C) Dendrograms show frequency
742 distribution of angle measurement.

743 **Figure 3. Rpsa KD is associated with defects in neuronal morphogenesis at P15 that can be**
744 **rescued by Rpsa OE**

745 A) Neurons transfected via *in utero* electroporation at E15.5, scale bars = 50 µm B) One-way
746 ANOVA shows a significant difference ($F(3,76) = 7.024$, $p < 0.0005$). Tukey post hoc test shows
747 the mean number of dendrites is significantly lower for Rpsa CRISPR group (2.9 ± 0.240,) as
748 compared to control CRISPR (4.2 ± 0.236) (p=0.002). There was no significant difference
749 between Rpsa CRISPR + Rpsa OE (4.0 ± 0.205) and control CRISPR + control tdTomato OE
750 groups (4.3 ± 0.301) (p= 0.751). For all groups n=20 cells from 3 mice. Data are represented as
751 mean ± SEM. C) One-way ANOVA shows significant difference ($F(3,76) = 24.361$, $p < 0.0005$).
752 Tukey post hoc test shows dendrite length is significantly lower for Rpsa CRISPR group (20.90
753 ± 2.04) as compared to control CRISPR (49.51 ± 2.19) (p<0.0005). There was no significant
754 difference between Rpsa CRISPR + Rpsa OE (45.29 ± 2.75) and control CRISPR + control
755 tdTomato OE groups (39.99 ± 3.31) (p=0.992). For all groups n=20 cells from 3 mice. Data are
756 represented as mean ± SEM. D) Sholl analysis shows a decrease in branching complexity in
757 Rpsa deficient cells that can be rescued by Rpsa OE. For all groups n=20 cells from 3 mice.

758 **Figure 4. Rpsa KD, PEDF KD, and Itga6 KD result in similar defects in neuronal**
759 **morphology and Rpsa OE and Itga6 OE can both rescue morphological defects after PEDF**
760 **KD by increasing the expression of Rpsa on the plasma membrane**

761 A) Neurons transfected via *in utero* electroporation at E15.5, scale bars = 50 µm. B) One-way
762 ANOVA determined there was a statistically significant difference ($F(7,152) = 12.211$, $p <$
763 0.0005). Tukey post hoc test revealed that mean number of dendrites was statistically
764 significantly lower for Rpsa CRISPR (2.9 ± 0.240) as compared to control CRISPR (4.2 ± 0.236)
765 (p=0.002) and that mean number of dendrites was statistically significantly lower for PEDF

766 shRNA (2.55 ± 0.211, $p<0.0005$) and Itga6 shRNA groups (2.50 ± 0.235, $p<0.0005$) as
767 compared to the control CRISPR (4.21 ± 0.249). There was no statistically significant difference
768 in mean number of dendrites between the PEDF shRNA + Rpsa OE (4.15 ± 0.167, $p=0.999$) and
769 PEDF shRNA + Itga6 OE (3.90 ± 0.204, $p=0.874$) as compared to the scramble shRNA + control
770 OE group (4.35 ± 0.302). For all groups n=20 cells from 3 mice. Data are represented as mean ±
771 SEM. C) One-way ANOVA determined there was a statistically significant difference ($F(7,152)$
772 $= 16.134$, $p < 0.0005$). Tukey post hoc test revealed that mean dendrite length was statistically
773 significantly lower for Rpsa CRISPR (20.90 ± 2.04) as compared to control CRISPR (49.51 ±
774 2.19) ($p<0.0005$) and that mean dendrite length was statistically significantly lower for PEDF
775 shRNA (27.04 ± 2.56, $p<0.0005$), and Itga6 shRNA (26.23 ± 3.30, $p<0.0005$) groups, as
776 compared to the scramble shRNA group (50.86 ± 3.56). There was no statistically significant
777 difference between PEDF shRNA + Rpsa OE (48.99 ± 3.569, $p=0.956$) and PEDF shRNA +
778 Itga6 OE (44.76 ± 3.366, $p=1.000$) as compared to the scramble shRNA + control OE group
779 (44.265 ± 3.307). For all groups n=20 cells from 3 mice. Data are represented as mean ± SEM.
780 D) Sholl analysis shows dramatic decrease in branching in Rpsa, PEDF, and Itga6 deficient cells
781 that is rescued in the PEDF shRNA + Rpsa OE and PEDF shRNA + Itga6 OE groups. For all
782 groups n=20 cells from 3 mice. E) Western blot showing Rpsa and Itga6 expression in the
783 nuclear, membrane, and cytosolic subcellular fractions.

784 **Figure 5. Rpsa KD and PEDF KD, but not Itga6 KD, cause a decrease in overall spine**
785 **density and a change in spine morphology**

786 A) Neurons transfected via *in utero* electroporation at E15.5, images taken with 63x objective
787 and 5x zoom to visualize spines, scale bares = 5 μm. B) One-way ANOVA determined there was
788 a statistically significant difference ($F(6,127) = 23.321$, $p < 0.0005$). Tukey post hoc test revealed

789 that mean spine density per μm was statistically significantly lower for Rpsa CRISPR (0.28 ±
790 0.04, n=21) as compared to control CRISPR (0.70 ± 0.05, n=12) (p=0.001) and mean spine
791 density per μm was statistically significantly lower for PEDF shRNA (0.21 ± 0.04, n=20) as
792 compared to scramble shRNA (0.97 ± 0.09, n=20) (p<0.0005). However, the Itga6 shRNA group
793 (1.01 ± 0.10, n=17) did not show a significant difference compared to the scramble shRNA
794 group (p=0.999). The PEDF shRNA + Rpsa OE group (0.99 ± 0.07, n=21) was not significantly
795 different from the scramble shRNA + control OE group (0.77 ± 0.08, n=20) (p=0.230). Data are
796 represented as mean ± SEM. For each group, spines were analyzed from 3 mice. C) Pie charts
797 showing the percentage of spines with filopodia, thin, stubby, mushroom, or branched
798 morphology for each experimental group.

799 **Figure 6. Calcium imaging shows sub-threshold functional difference in Rpsa KD neurons**
800 A) Mean difference in GCaMP6s fluorescence intensity. Two-tailed independent-samples t-test
801 showed the average difference between maximum and minimum peaks was significantly greater
802 in the control (12.79 ± 1.06, n=22 cells from 3 mice) compared to Rpsa KD (6.73 ± 1.80, n=19
803 cells from 3 mice), t(39) = 2.992, p = 0.035. Data are represented as mean ± SEM. B)
804 Representative % change in fluorescence ($\Delta F/F_0$) for representative individual neuron in mouse
805 brain slice. Single action potentials are defined as $\Delta F/F0 \geq 23\% \pm 3.2\%$. The left panels were
806 taken over 20 seconds and the right panels show a 5 second section of each representative trace,
807 with the y-axis measuring 8 units to provide a zoomed in view. C) Electrophysiology recordings
808 confirm low spontaneous firing rate of control CRISPR and Rpsa CRISPR neurons.
809 Representative traces of spontaneous activity of 3 control CRISPR and Rpsa CRISPR neurons at
810 resting membrane potential in current-clamp mode. n= 9 cells from 3 control CRISPR mice and
811 n= 7 cells from 2 Rpsa CRISPR mice.

812 **Figure 7. Schematic of Rpsa/PEDF/Itga6 signaling regulating neuronal morphogenesis**

813 A) Under normal conditions Itga6, which is likely bound to a β4 subunit to function as part of a
814 complete integrin, is co-localized on the plasma membrane with Rpsa. Both Rpsa and Itga6
815 facilitate the binding of PEDF to Rpsa, which results in signaling to regulate proper neuronal
816 morphogenesis (top left). Following Rpsa KD, PEDF KD, or Itga6 KD the signaling mechanism
817 initiated by Rpsa is attenuated, resulting in severe defects in morphology (top right). Knockdown
818 of the upstream ligand PEDF can be compensated for by increasing its downstream receptor
819 Rpsa, to cause increase of Rpsa-Itga6-Itgb4 complex, thus resulting in normal level of signal
820 intensity and normal morphogenesis. The increase in Rpsa-Itga6-Itgb4 complex can also be
821 accomplished by Itga6 OE (bottom). B) Two potential mechanistic explanations for the increase
822 in Rpsa expression on the plasma membrane following Itga6 OE. Rpsa and Itga6 may bind each
823 other in the cytoplasm and co-localize to be trafficked to the plasma membrane together (top).
824 Rpsa and Itga6 may independently express on the plasma membrane and then form a complex to
825 allow stabilization of Rpsa via Itga6 (bottom).

826 **Supplemental Figure 1. Validation of KD plasmids**

827 A) Western blots showing the efficacy of Rpsa KD, PEDF KD, and Itga6 KD done using 293T
828 and COS-1 cells. B) Quatification of Western blots done using ImageJ shows Rpsa CRISPR
829 efficiency is ~77%, PEDF shRNA efficiency is ~84%, and Itga6 shRNA efficiency is ~ 79%.
830 Three biological/technical replicates were used (n = 3). Band intensity was quantified and
831 normalized to GAPDH. C) Representative chromatograms for the target sequence of Rpsa
832 CRISPR. D) Representative Rpsa gene alterations caused by Rpsa CRISPR. Numbers indicate
833 amino acid position in Rpsa protein. Sequences in red font show the target of Rpsa gRNA and
834 PAM sequence. E) Immunofluorescence staining of cortical primary neurons transfected with

835 pCAG-eCas9-GFP-U6-Rpsa-gRNA plasmid upon plating and then fixed after 6 days in culture.
836 Note that in the GFP-positive Rpsa KD neuron Rpsa staining is reduced compared to
837 surrounding GFP-negative normal neurons. Scale bar = 50 μm. F) Quantification of Rpsa marker
838 fluorescence intensity. Rpsa corrected total cell fluorescence (CTCF) is significiantly decreased
839 in neurons positive for Rpsa CRISPR (43,881.13 CTFC ± 5,156.70), as compared to
840 untransfected controls (85,504.51 CTFC ± 9,189.28), $t(38) = 3.950$, $p<0.0005$.

841 **Supplemental Figure 2. Dendrite length at P3 after Rpsa KD**

842 *In utero* electroporation was performed at E15.5. One-way ANOVA determined there was no
843 statistically significant difference in dendrite length between Rpsa CRISPR (27.68 ± 1.40) and
844 control CRISPR (27.53 ± 1.56) at P3 ($F(3,96) = 0.503$, $p = 0.681$). For all groups, n=25 cells
845 from 3 mice. Data are represented as mean ± SEM.

846 **Supplemental Figure 3. Intrinsic properties of neurons in *ex vivo* brain slice preparation**

847 Control CRISPR and Rpsa CRISPR neurons display similar intrinsic membrane properties. A)
848 Examples of a control CRISPR and Rpsa CRISPR neuron responding to a series of
849 hyperpolarizing and depolarizing current steps from a holding potential of −65 mV. B)
850 Quantification demonstrated that capacitance was significantly larger in the Rpsa CRISPR group.
851 No other significant differences in membrane properties were found between the control
852 CRISPR (n= 9 cells from 3 mice) and the KD group (n=7 cells from 2 mice).

Figure 1. **Blazejewski et al.**

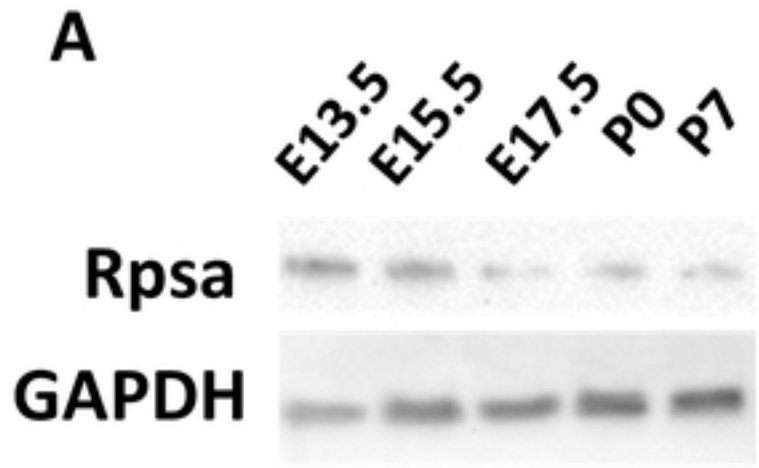

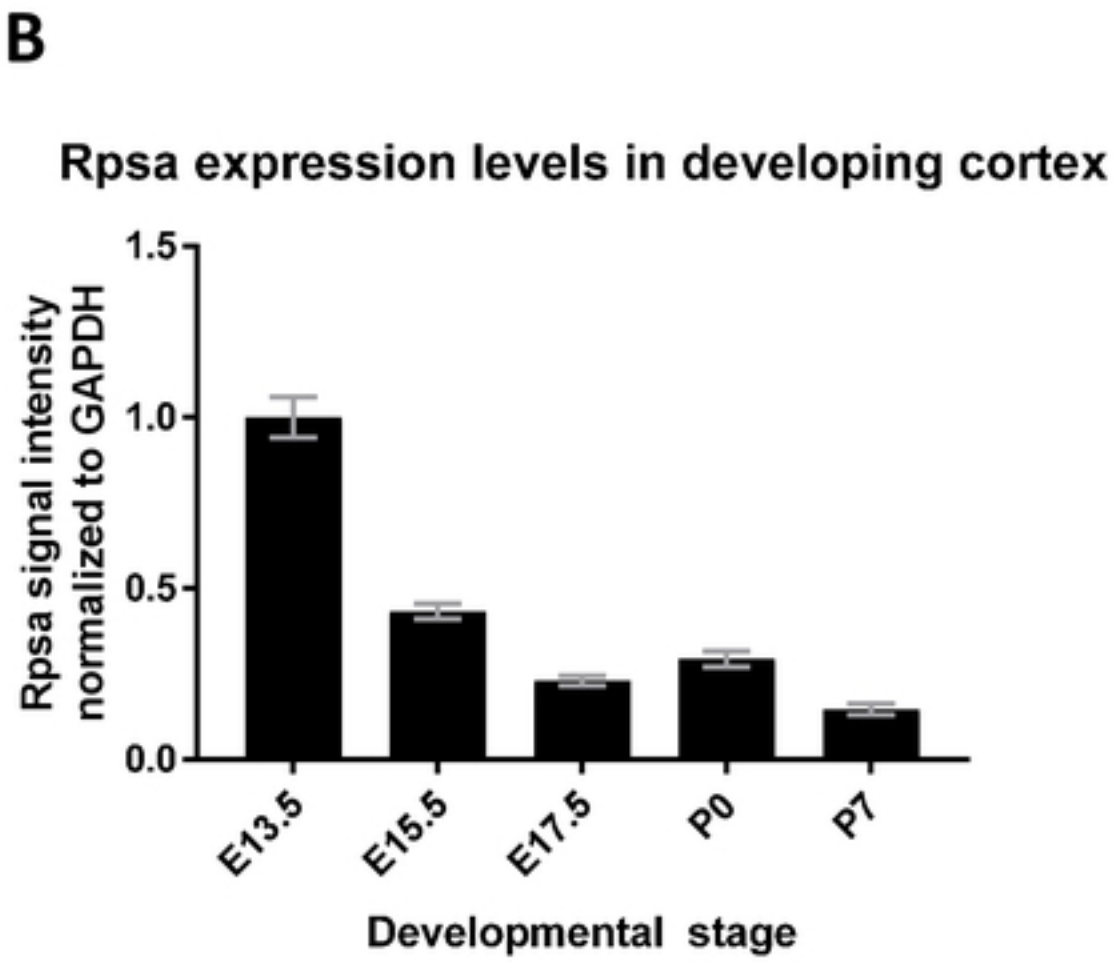

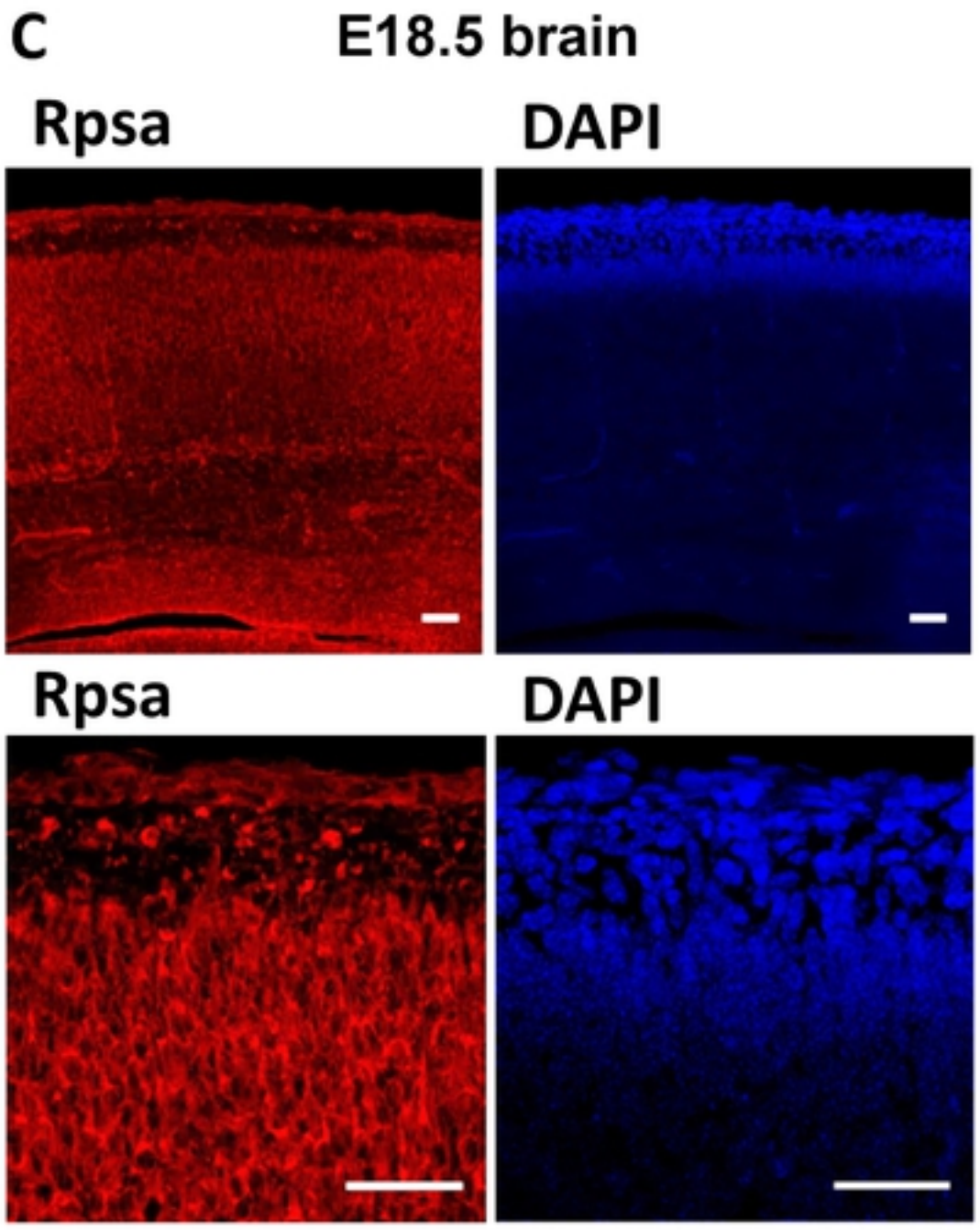

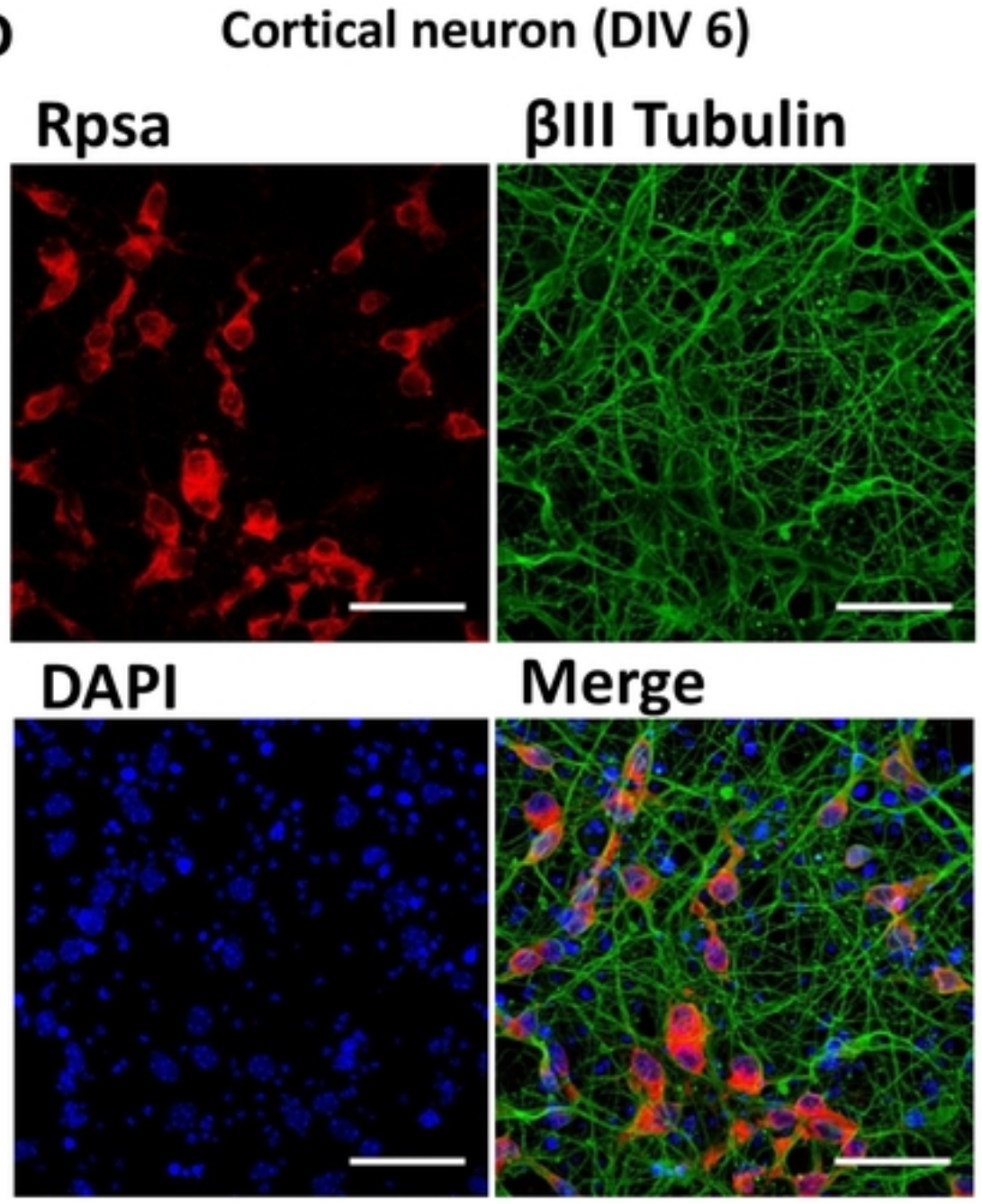

Figure 2.

Blazejewski et al.

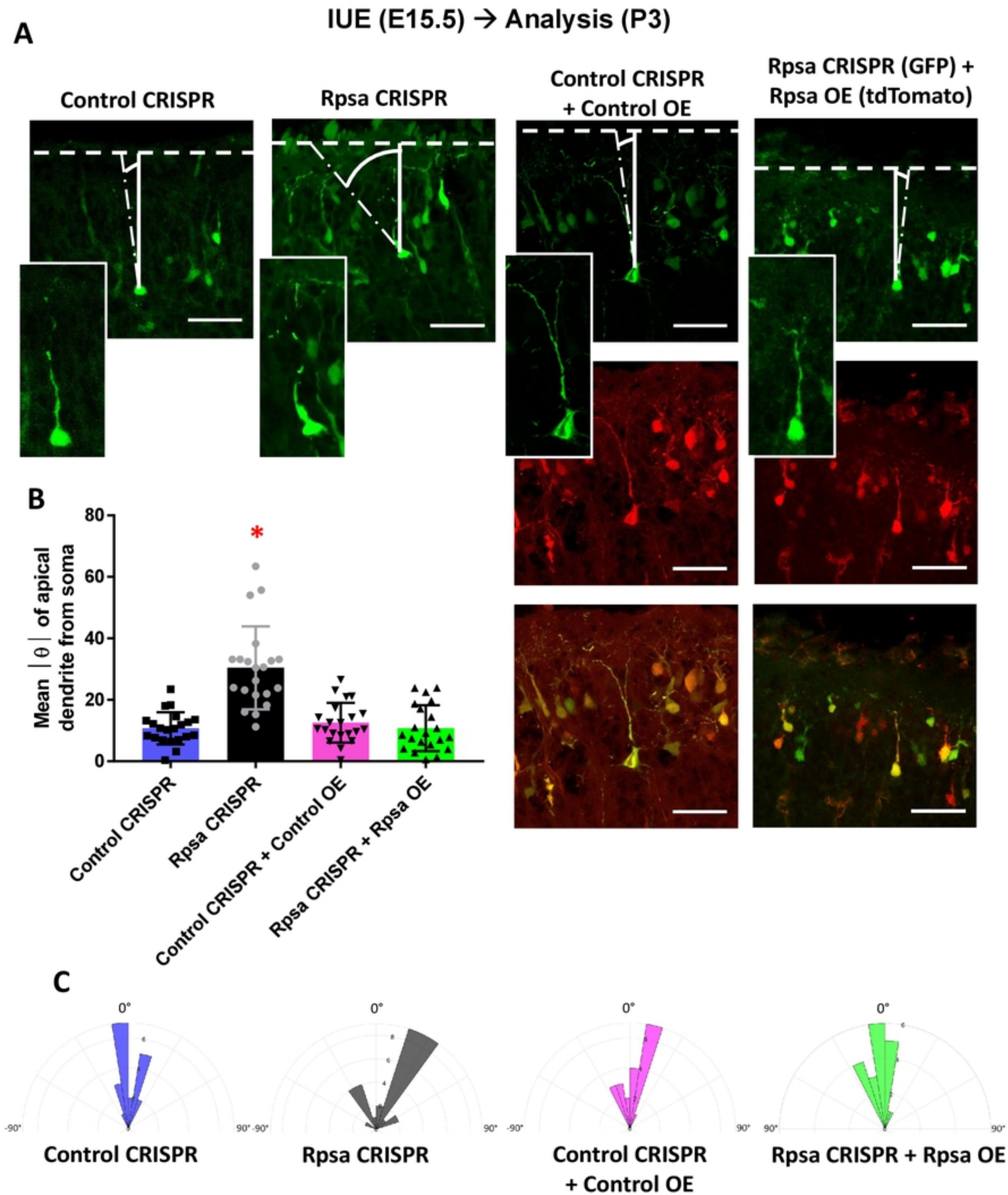

Figure 3.

Blazejewski et al.

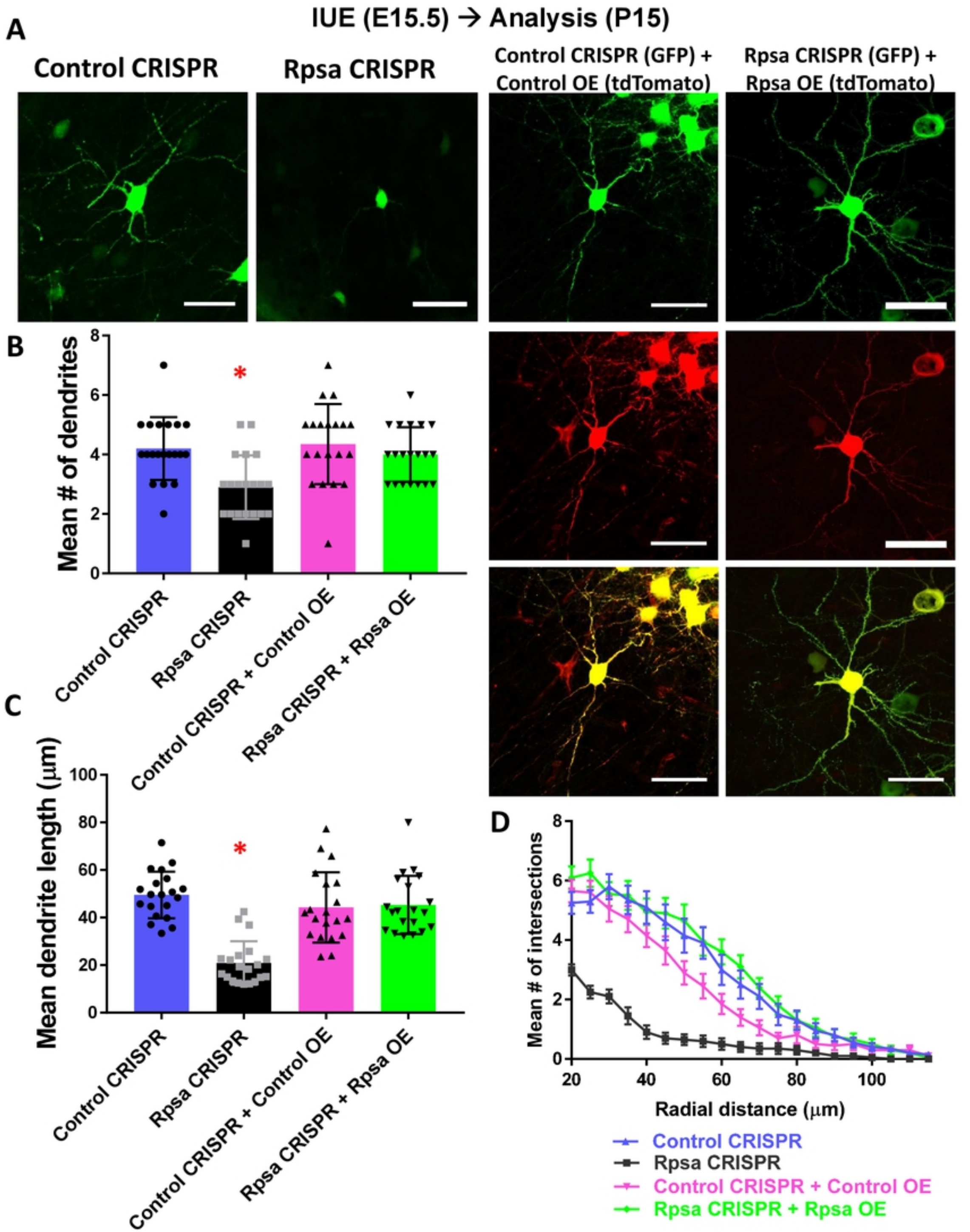

Figure 4.

Blazejewski et al.

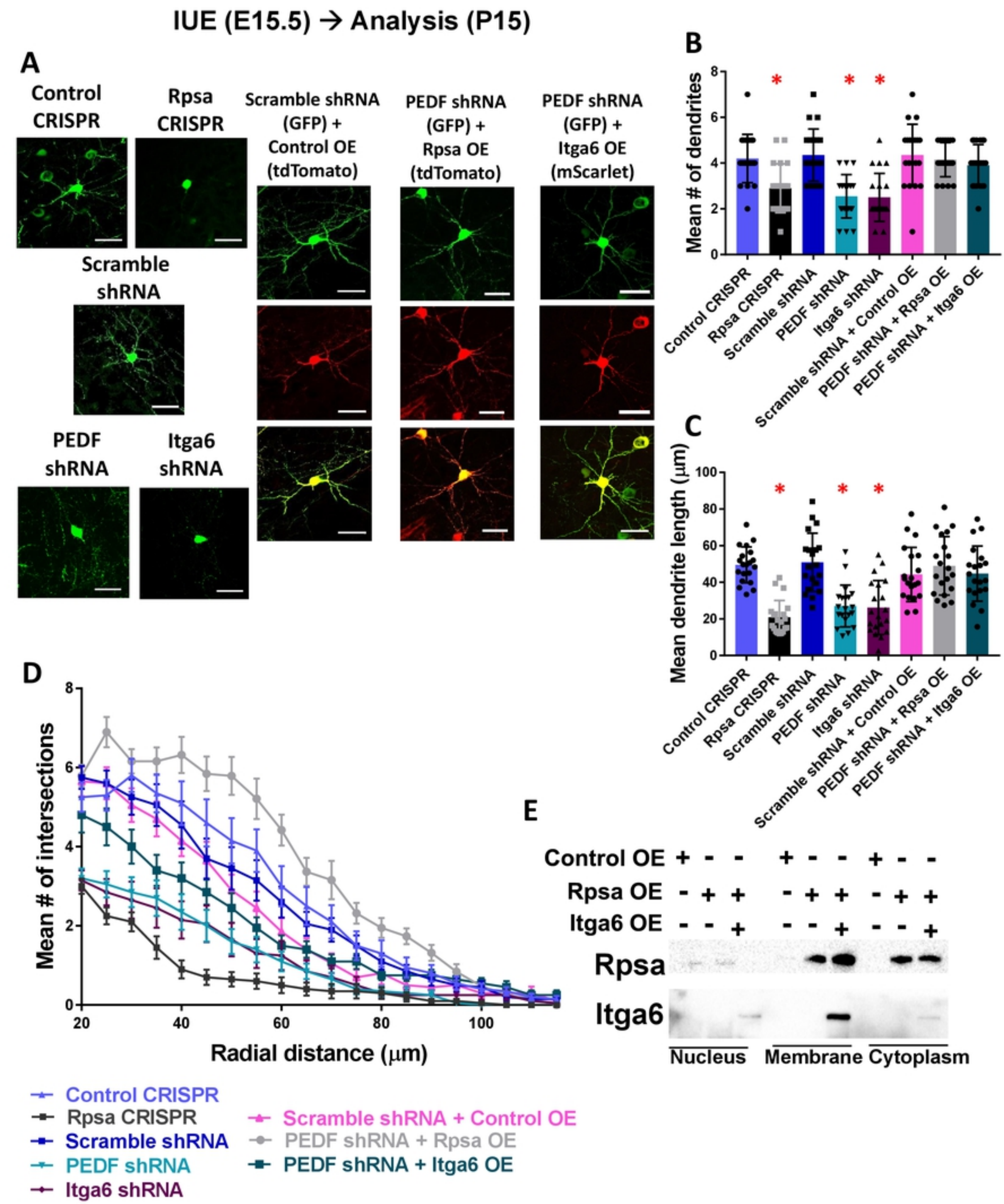

Figure 5.

Blazejewski et al.

A

IUE (E15.5) → Analysis (P15)

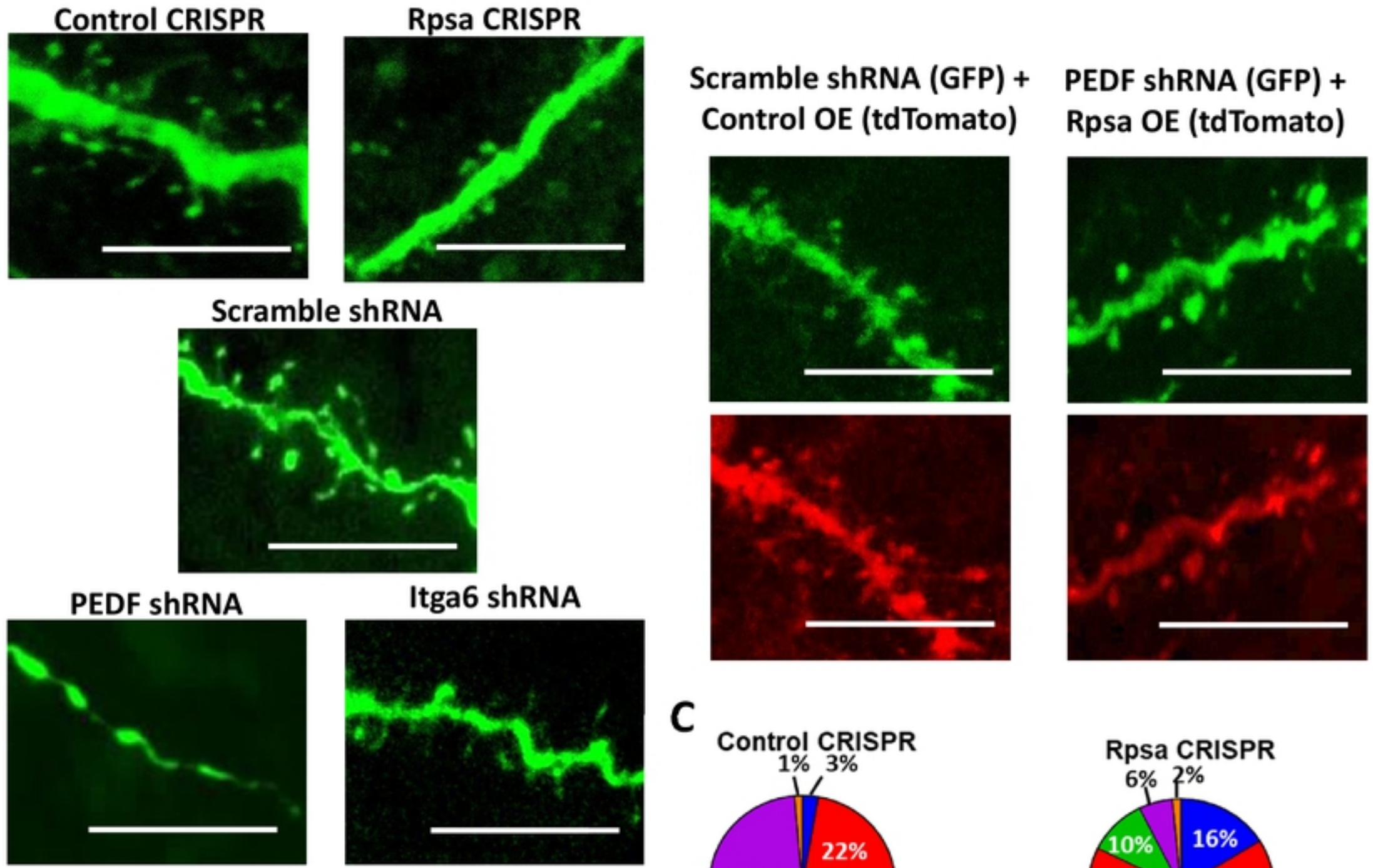

B

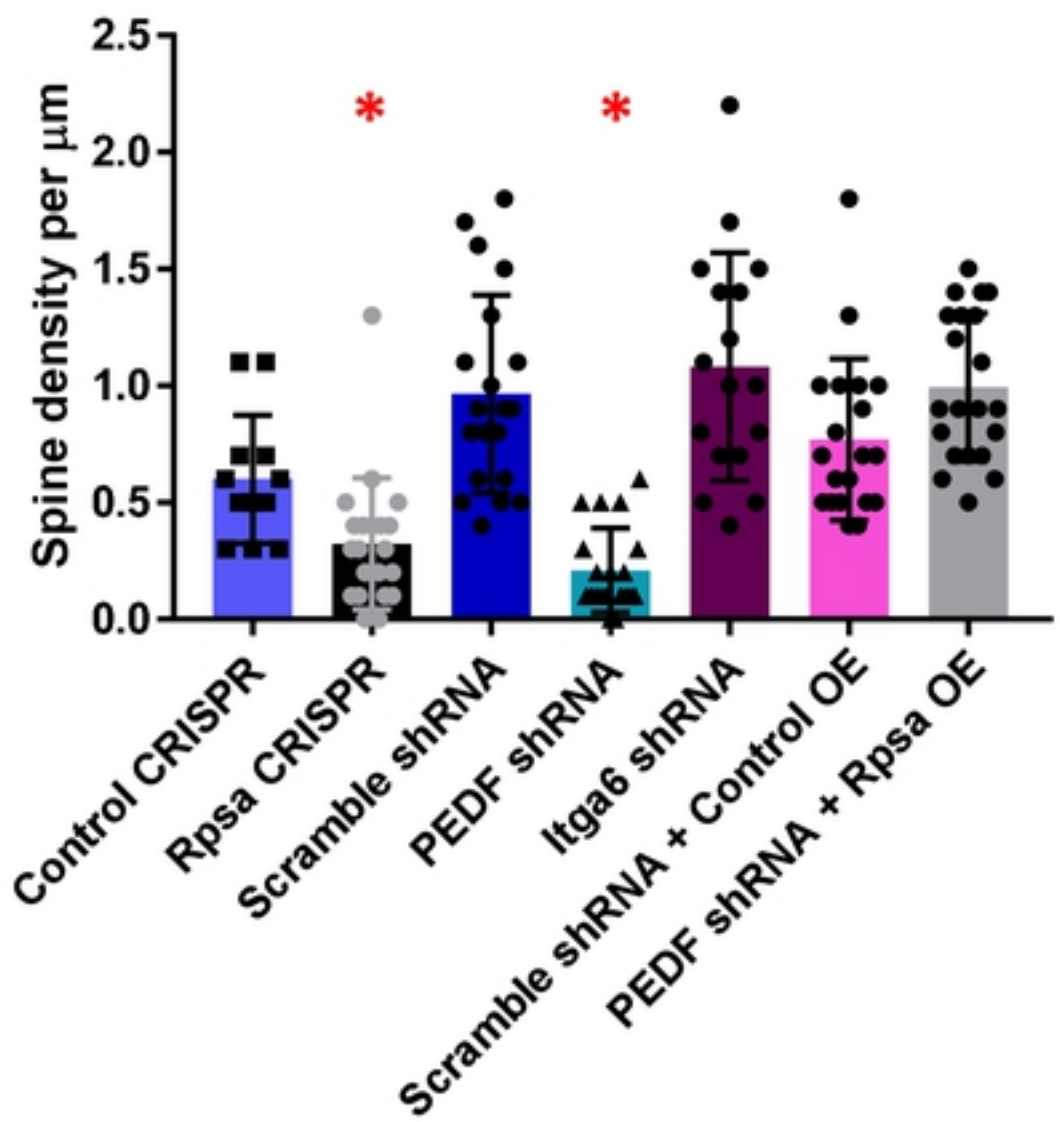

C

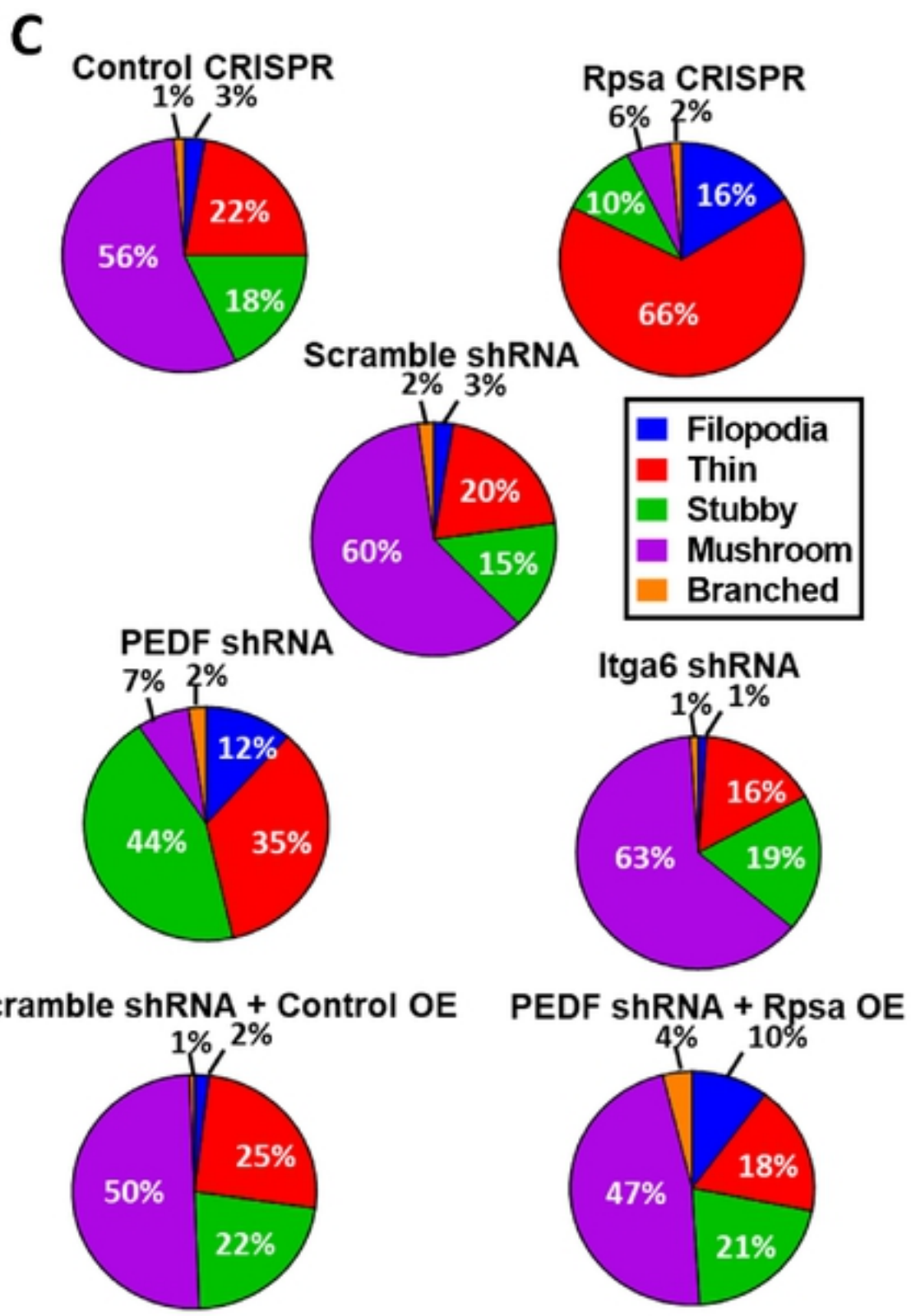

Figure 6. **Blazejewski et al.**

IUE (E15.5) → Analysis (P15-P60)

A

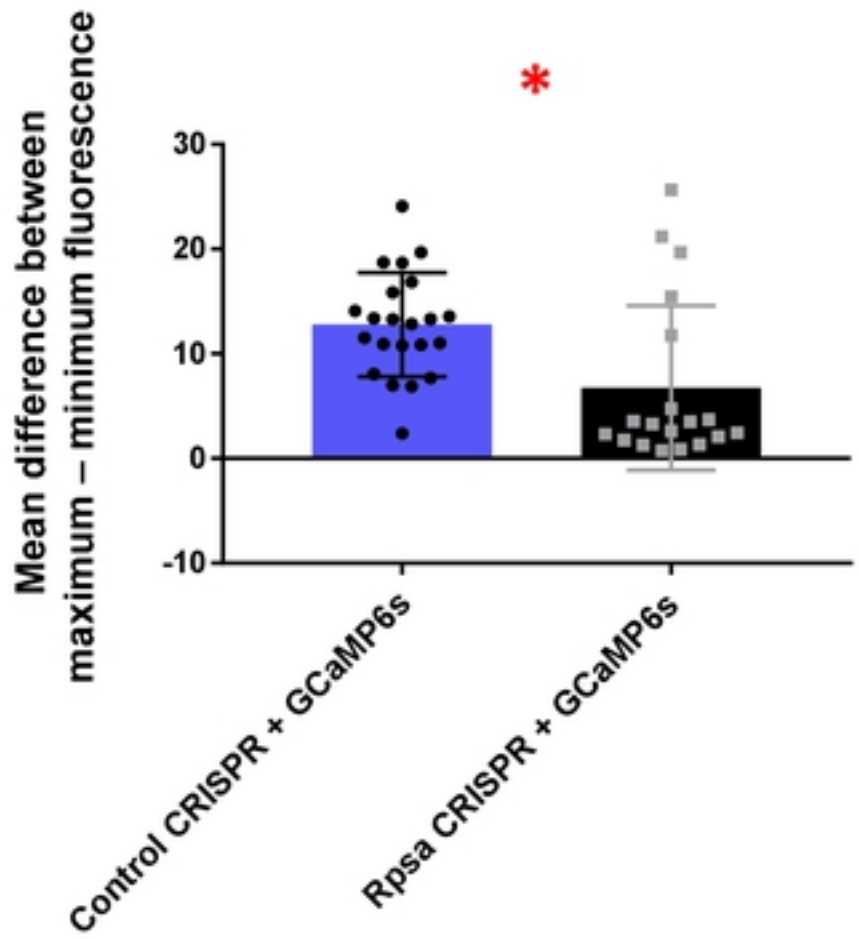

B

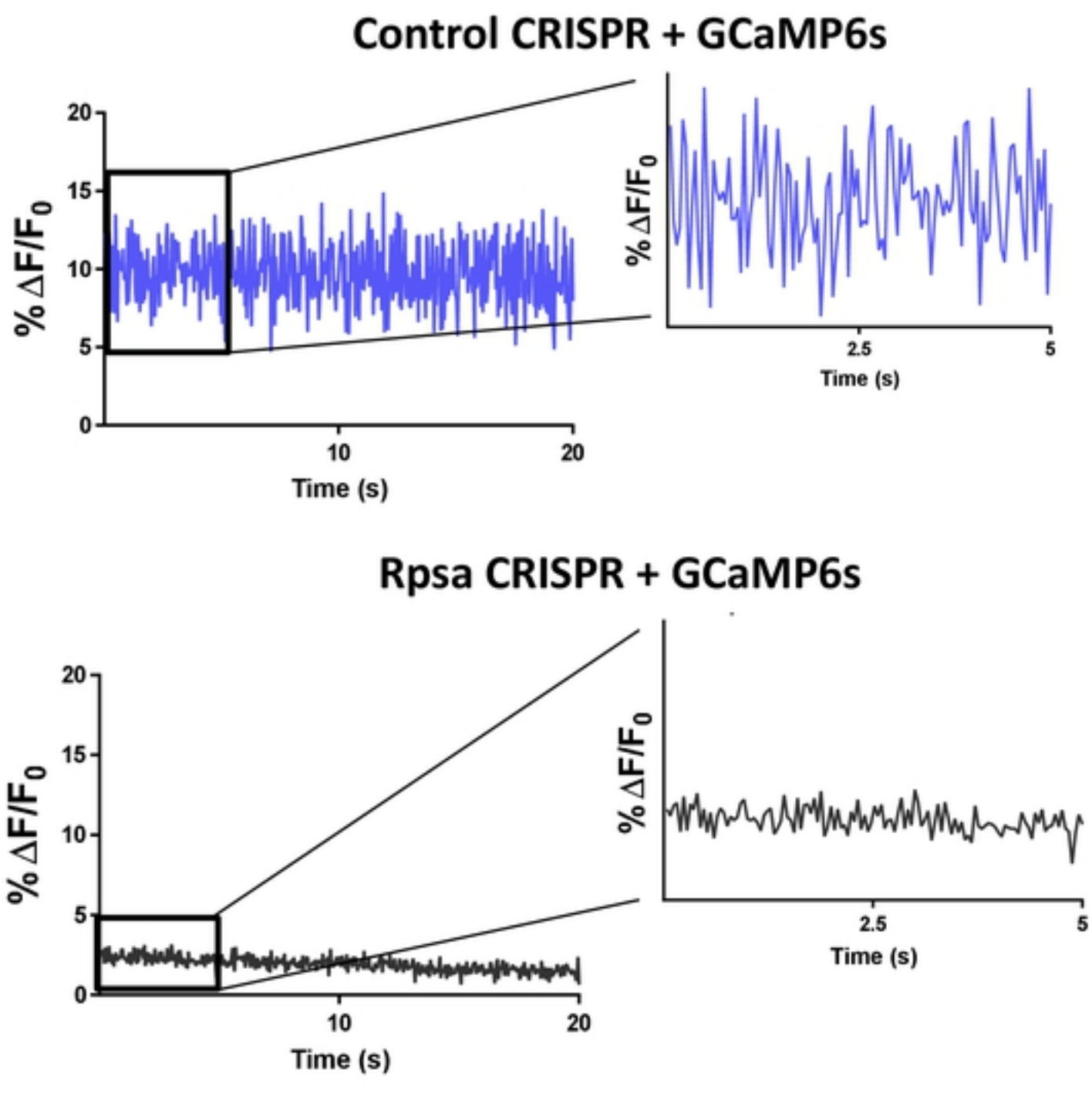

C

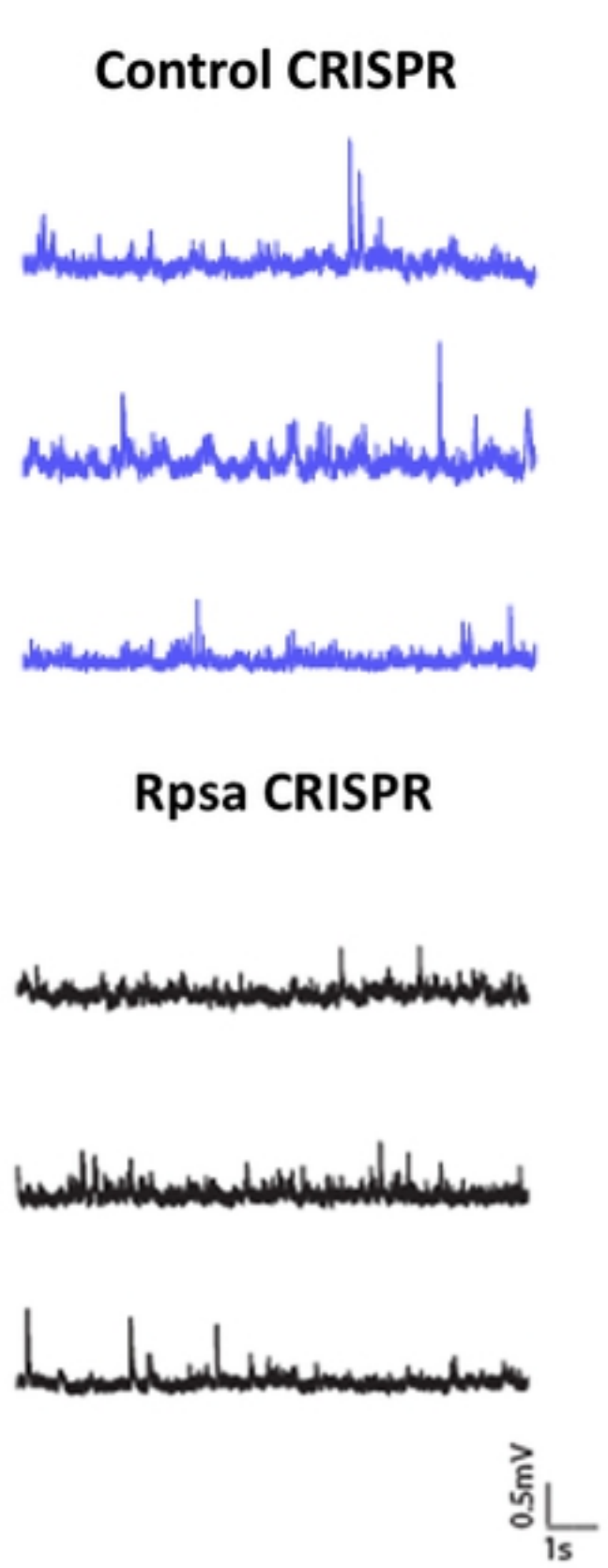

Figure 7.

Blazejewski et al.

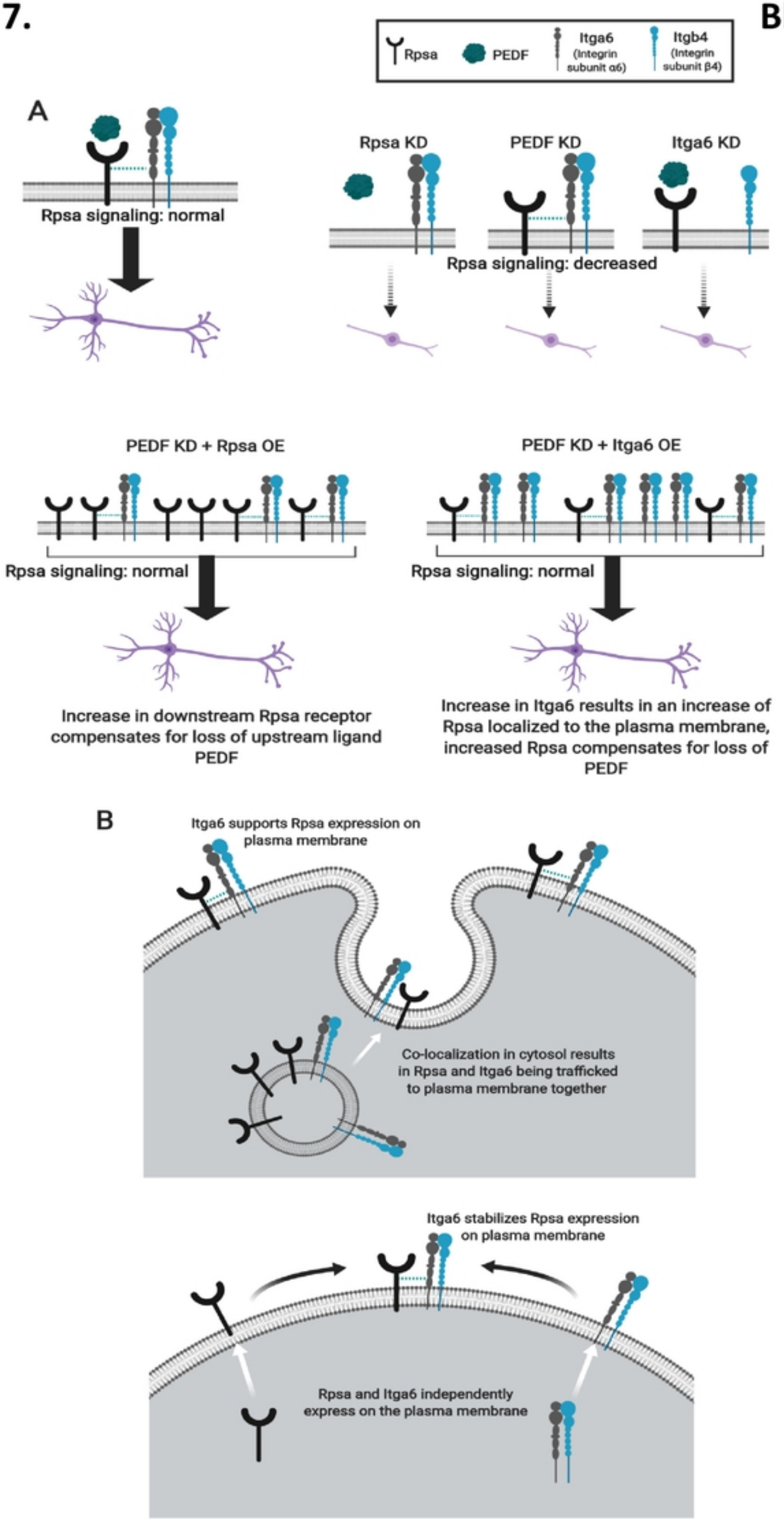

Supplemental Figure 1. **Blazejewski et al.**

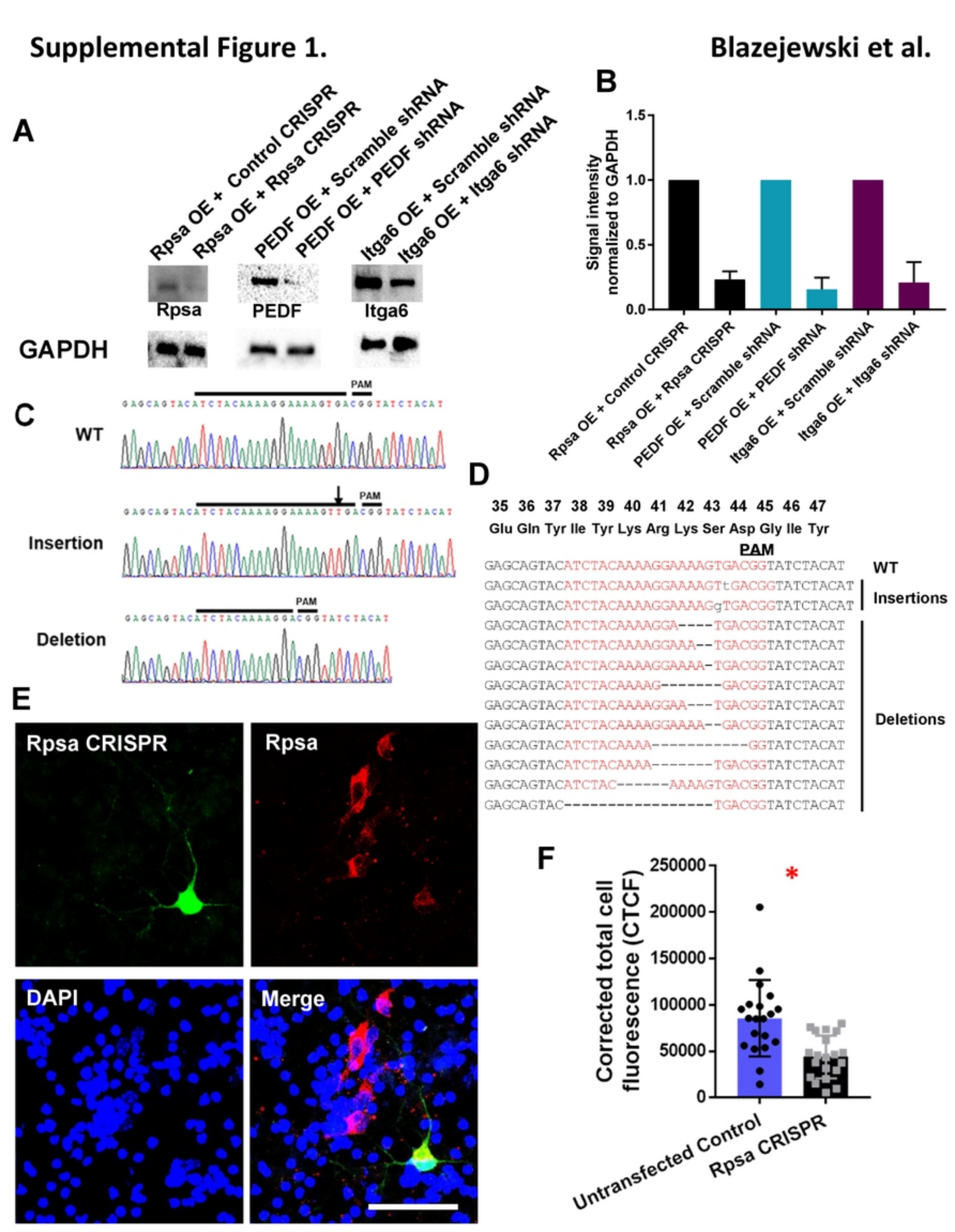

Supplemental Figure 2. **Blazejewski et al.**

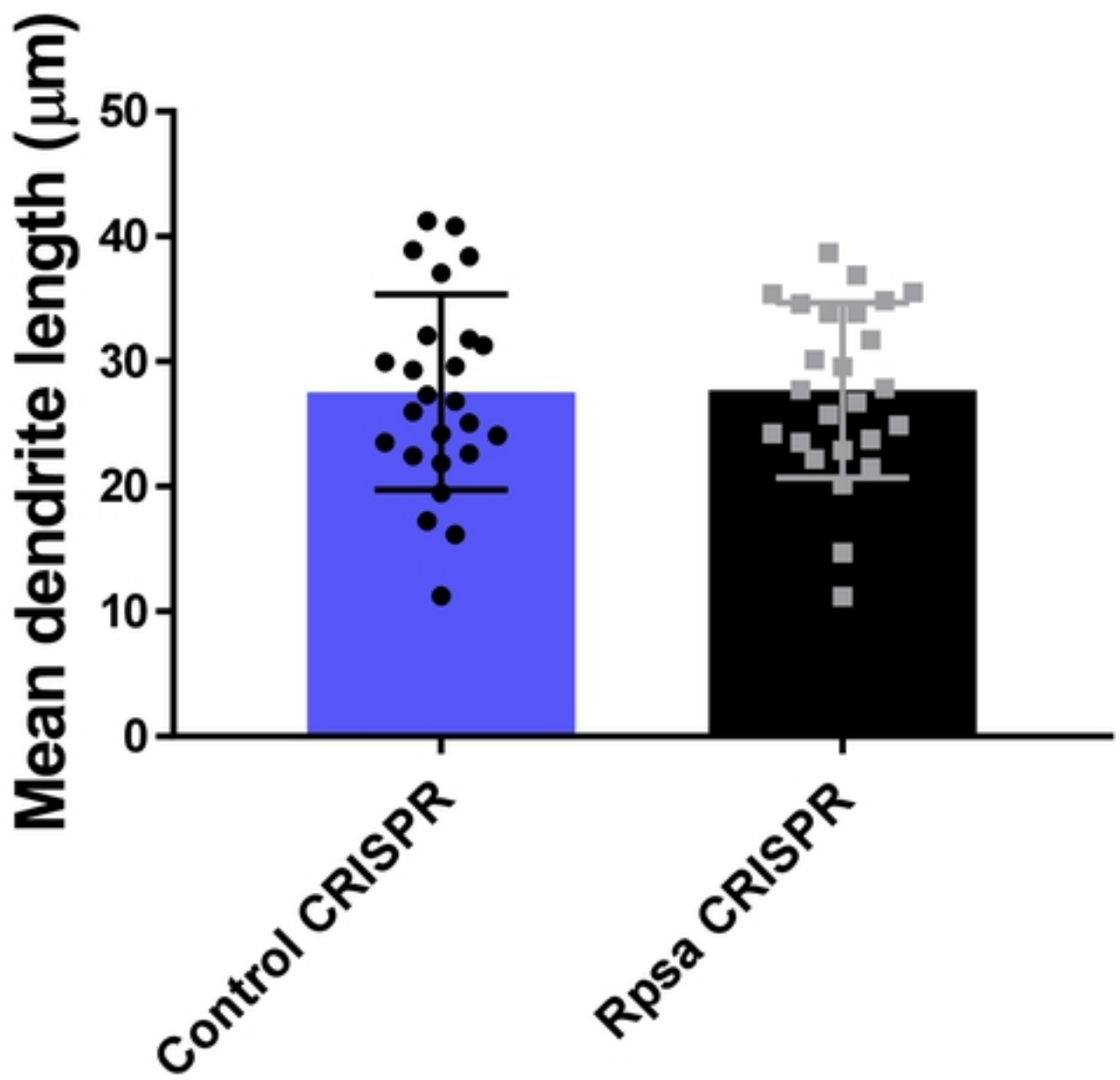

Supplemental Figure 3. **Blazejewski et al.**

A

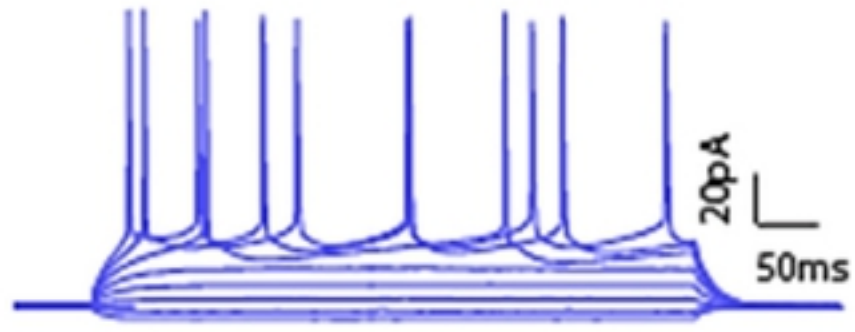
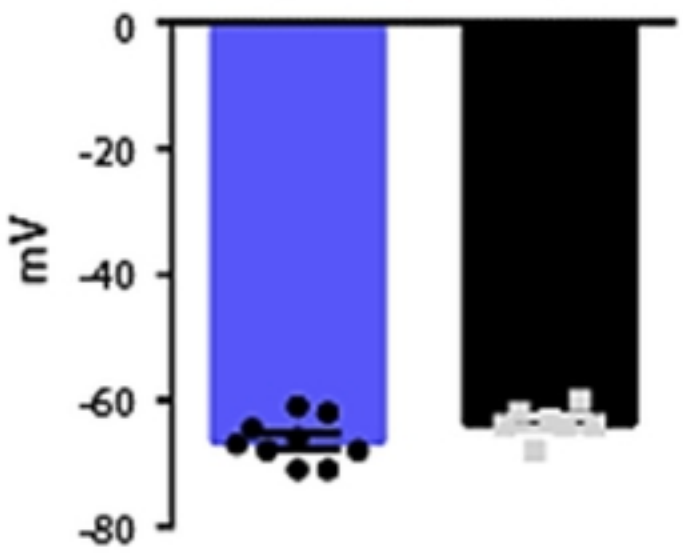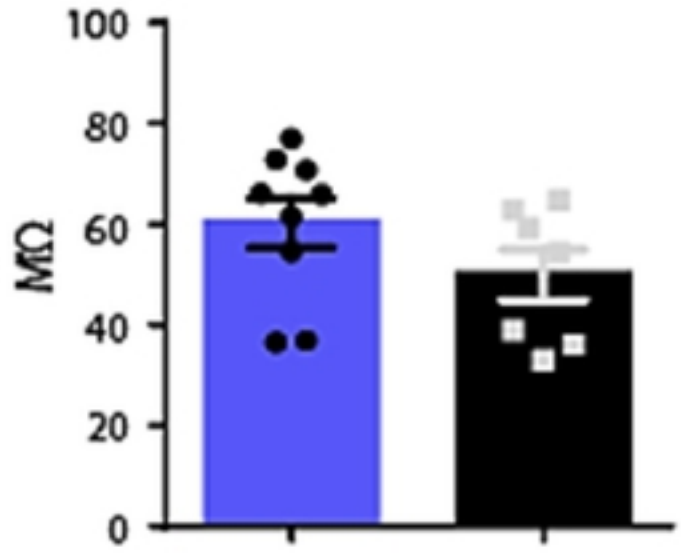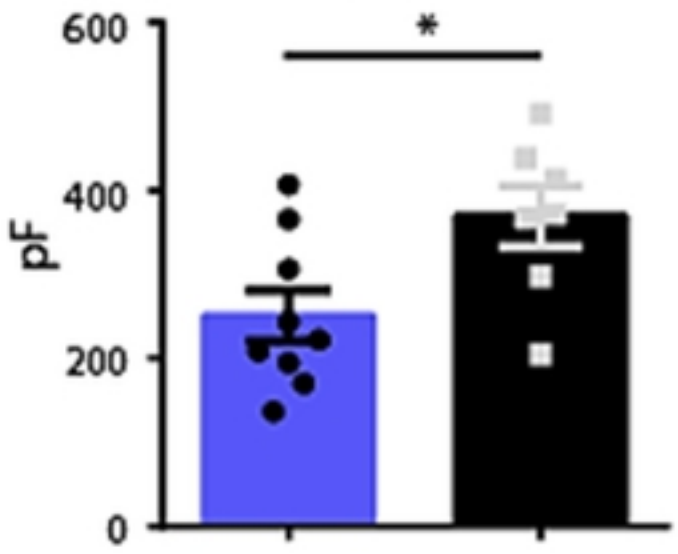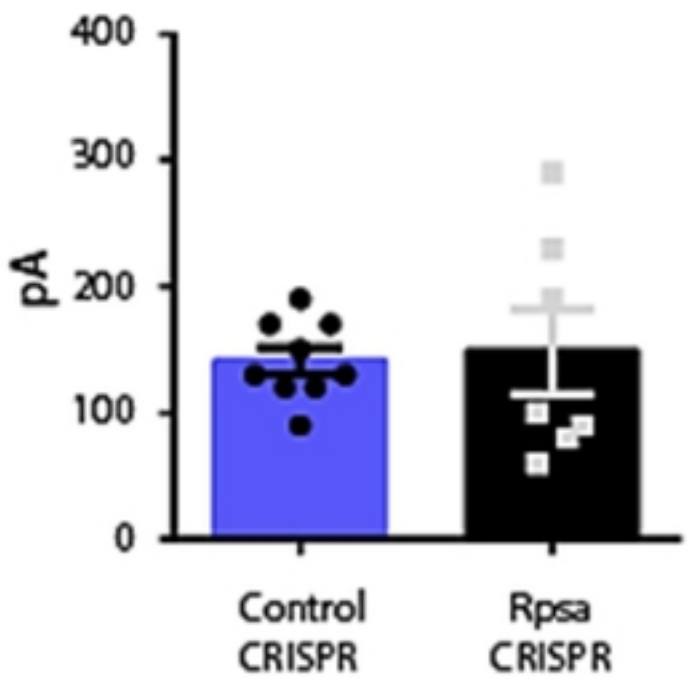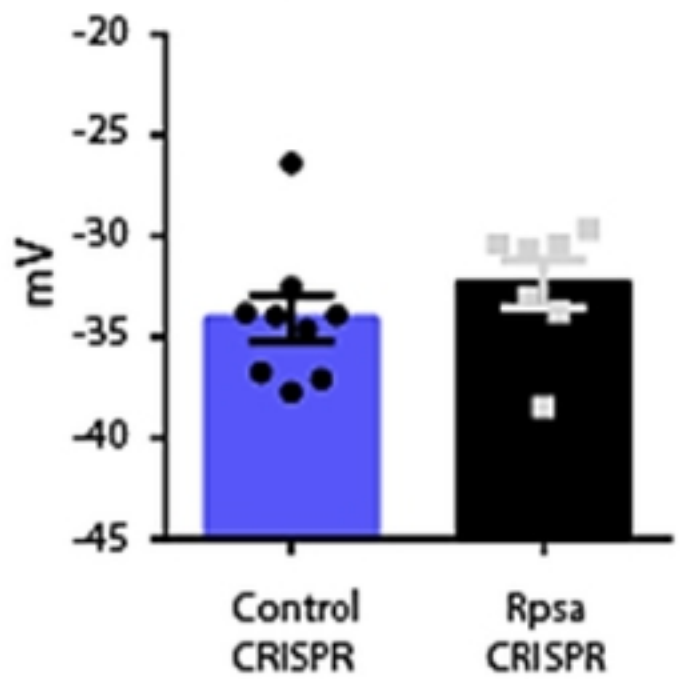
B